VOLTAGE CONTROLLED NON-VOLATILE SPIN STATE AND CONDUCTANCE SWITCHING OF A MOLECULAR THIN FILM HETEROSTRUCTURE

by

Aaron Mosey

A Dissertation

Submitted to the Faculty of Purdue University

In Partial Fulfillment of the Requirements for the degree of

Doctor of Philosophy

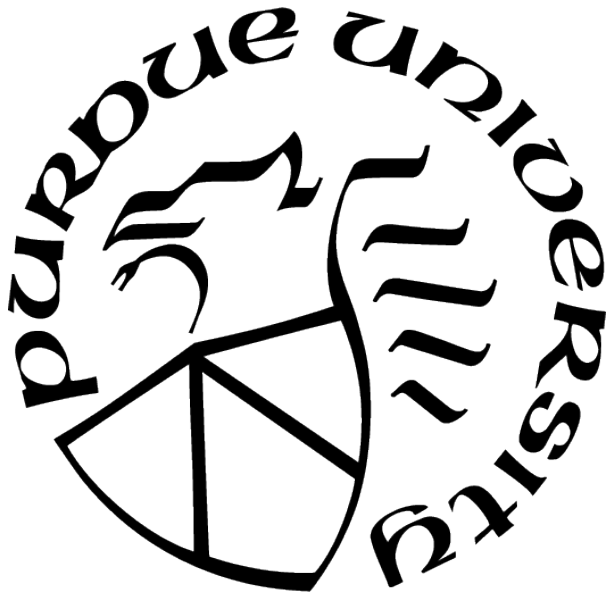

Department of Physics

Indianapolis, Indiana

May 2021

THE PURDUE UNIVERSITY GRADUATE SCHOOL
STATEMENT OF COMMITTEE APPROVAL

Dr. Ruihua Cheng, Chair

Department of Physics

Dr. Gabor Csathy

Department of Physics

Dr. Ricardo Decca

Department of Physics

Dr. Yogesh Joglekar

Department of Physics

Dr. Gautam Vemuri

Department of Physics

Approved by:

Dr. Ricardo Decca

For those willing to take risks

ACKNOWLEDGMENTS

George Mosey for Perseverance

Janie (Holliday) Mosey for Gentleness and Gratitude

Nathalie my bride for Unconditional Love and Support

Hoyt Tye for Resourcefulness and Spirit

Jimmy K., Dottie G. and Friends for Precedence

Nate Rush for Purpose

Craig White for Commitment

Petra Batek for Guidance

IUPUI Department of Physics for Knowledge, Structure, and Opportunity

Doc Holliday for the proper genetics.

TABLE OF CONTENTS

LIST OF FIGURES

ABSTRACT

Thermal constraints and the quantum limit will soon put a boundary on the scale of new micro and nano magnetoelectronic devices. This necessitates a push into the limits of harnessable natural phenomena to facilitate a post-Moore's era of design. Requirements for thermodynamic stability at room temperature, fast (Ghz) switching, and low energy cost narrow the list of candidates. Molecular electronic frontier orbital structure of some d-block transition metal ions in crystal fields will deform in response to their local energetic environment, giving rise to the e_g and t_{2g} suborbitals. More specifically, in an mononuclear Fe(II) complex, the energetic scale between these two orbitals yields an S=0 low spin diamagnetic state and an S=2 high spin paramagnetic state. Spin crossover complex $[Fe\{H_2B(pz)_2\}_2(bipy)]$ will show locking of its spin state well above the transition temperature, with an accompanied change of conductivity, when placed in a polar environment. Here we show voltage controllable, room temperature, stable locking of the spin state, and the corresponding conductivity change, when molecular thin films of $[Fe\{H_2B(pz)_2\}_2(bipy)]$ are deposited on a ferroelectric polyvinylidene fluoride hexafluropropylene substrate. This opens the door to the creation of a thermodynamically stable, room temperature, molecular multiferroic gated voltage device.

1. INTRODUCTION

Thermal constraints and the quantum limit will soon put a boundary on device technology[1], [2]. This limitation is the impetus which drives much research today [3]–[6], bringing with it a new motivation to probe natures secrets. In order to push past these limits into a post-Moore's era, a new generation of magneto-electric materials are needed. Molecular organic spintronics are one such material candidate[7].

This work outlines a research project which involves an isothermal coupling of the spin crossover phenomena by octahedral coordination complex $[Fe\{H_2B\,(pz)_2\}_2\,(bipy)]\,(pz = pyrazol-1-yl, bipy = 2,2-bipyradine)$ to a ferroelectric substrate of the homopolymer polyvinlyidene flouride (PVDF) $-\,(CH_2CF_2)\,-$ and it's copolymer poly(vinylidene flouride-co-hexafluoropropylene) $(-CH_2CF_2-)_x\,[-CF_2CF\,(CF_3)\,-]_y$, its subsequent effects on electrical transport properties, and an analysis of the energy involved in switching between the two distinct spin states. End to end fabrication of the multilayered structure including; magnetron sputtering, thermal evaporation, Langmuir-Blodgett layer by layer deposition, and relevant conditioning processes will be discussed, as well as characterization techniques such as; X-ray Absorption Spectroscopy (XAS), X-ray diffraction (XRD), ferroelectric characterization, atomic force microscopy, and low current conductivity testing. The end goal of this project is the creation of a novel, organic, molecular-based, multiferroic gated electronic device, which is nonvolatile and thermodynamically stable at room temperature.

1.1 The spin crossover molecule $[\mathbf{Fe\{H_2B\,(pz)_2\}_2\,(bipy)}]$

Octahedral ligand field surroundings of a single Fe(II) ion produce a spin bistability, the state of which is dependent upon external thermodynamic constraints. The frontier orbital of the central Fe ion is subject to distortions, giving rise to well known splitting into the e_g and t_{2g} molecular sub-orbital configuration, and subsequent Low Spin (LS) diamagnetic, or High Spin (HS) paramagnetic, electron spin configuration. The nature of this split is dictated by an energy difference determined by the distortion, and hence external thermo-

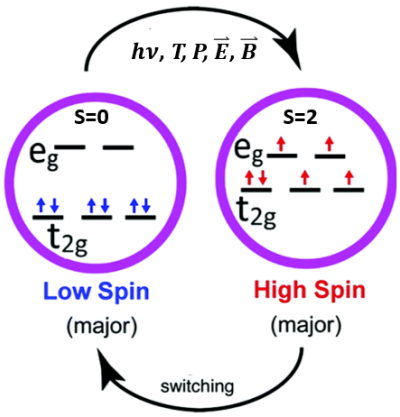

Figure 1.1. Spin crossover in an Fe(II) octahedral coordination compound is contingent upon the energetic splitting of the e_g and t_{2g} orbitals, which is dictated by the local environment of the molecule and can be altered by light, temperature, pressure, electric field, and magnetic field.

dynamic conditions. Summed up pictorially in Figure 1.1, these conditions are pressure, light, temperature, magnetic field, and electric field.

The strength of the interaction of the ligand field with the d orbital of the central transition metal ion will dictate the energetic splitting of the suborbitals and is expressed as the semi-empirical parameter $10Dq$ [8]. In turn, this gives rise to an environment which would energetically favor following Hund's rules for the electronic population of the molecular suborbitals, or not. The determining threshold for this energy difference is on the order of the spin pairing energy [9]. For a d^6 transition metal ocathedral coordination complex this energy, Π, may be given by

$$\Pi = 2\tfrac{1}{2}B + 4C \tag{1.1}$$

where B and C are the Racah parameters [10] for electron-electron Coulombic repulsion. A complete treatment for the physical basis of the molecular orbital splitting is given in *Chapter 2: Background and Theoretical* section of this report.

1.1.1 The structure of $[\mathbf{Fe\{H_2B\,(pz)_2\}_2\,(bipy)}]$

The spin crossover molecule $[Fe\{H_2B\,(pz)_2\}_2\,(bipy)]$ consists of a central Fe(II) ion double bonded to two pyrazole ($C_3H_4N_2$) ligands and one 2,2'-bipyridine ($C_{10}H_8N_2$) ligand. Generally speaking, it is the length of double bonds to the 2,2'-bipyridine which dictate the strength of the ligand field interaction with the d orbitals of the central Fe ion. A shorter bond length corresponding to a stronger interaction, tending towards the $S = 0$ LS state, longer bond length a weaker interaction which tends to an $S = 2$ HS state. In a bulk sample, of course there will be a mixture of the two states. As is convention, we will denote the ratio of this mixture γ, with the appropriate subscript HS or LS, HS for the ratio of HS:LS, and LS for the ratio LS:HS. When $\gamma_{HS} = \gamma_{LS}$ the system is said to be at the transition point. The temperature at which this occurs is known as the transition temperature and is denoted by $T_{1/2}$. Spin crossover in $[Fe\{H_2B\,(pz)_2\}_2\,(bipy)]$ exhibits hysteresis and is the result of a nucleation and growth process, it is a first-order spin transition showing cooperativity [11].

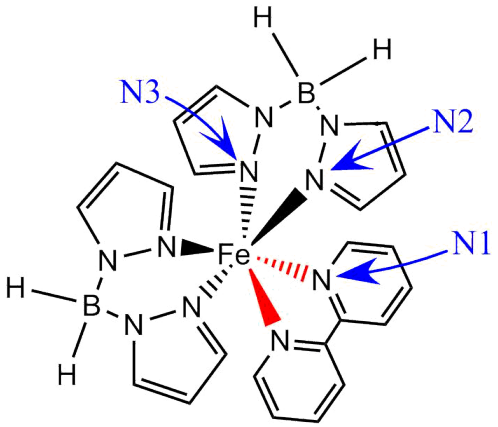

Figure 1.2. The structure of $[Fe\{H_2B\,(pz)_2\}_2\,(bipy)]$. The double bonds to the monodentate 2,2'-bipyridine ligand are highlighted in red. It is the length of these bonds that is primarily responsible for the strength of the ligand field interaction, and thus the amount of distortion of the Fe's d orbital, resulting in the spin crossover phenomena.

Crystallites of $[Fe\{H_2B\,(pz)_2\}_2\,(bipy)]$ have monoclinic crystal structure of space group C2/c, with lattice constants $a = 16.307(2), b = 15.075(4), c = 11.024(4)$, and $\beta = 114.95(5)°$ at 293K [12]. A representative bond diagram of the molecule is shown in Figure 1.2. The

central Fe ion is bonded to nitrogen atoms from each of its ligands. Taking N1 to be a member of the bipyridene ligand and N2 and N3 to be members of the pyrazole ligands, the Fe-N1 bond length is 2.213 Å, Fe-N2 is 2.190 Å, and Fe-N3 is 2.157 Å. Considering room temperature geometry N1-Fe-N2, N3-Fe-N1, and N3-Fe-N2 have respective bond angles of 93.1°, 97.2°, and 88.7°.

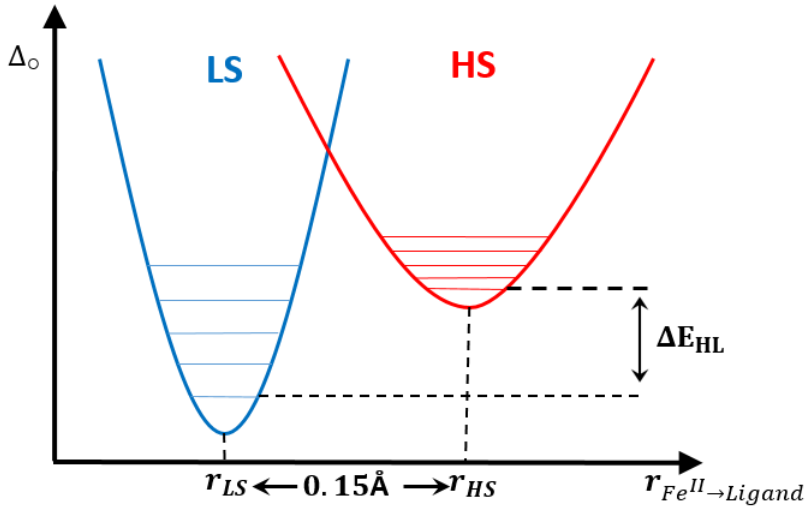

Figure 1.3. The energetic difference between the HS S=2 and LS S=0 states as a function of ligand to ion distance. As the ligands move closer to the ions, electrons are more likely to populate only the LS state.

The spin crossover transition is a result of dynamic behavior on the part of bond length structure change and ligand spatial orientation within the molecule. As the molecule dips below the transition temperature bond lengths change and the ligands rotate. This occurs primarily between the Fe ion and the 2,2'-bipyridine ligand, and to a lesser degree with the pyrazole ligands. At 139K we have new bond lengths as follows: the Fe-N1 bond is now 2.013 Å, Fe-N2 is 2.046 Å, and Fe-N3 is 2.039 Å, with new geometry for N1-Fe-N2, N3-Fe-N1, and N3-Fe-N2 at respective bond angles of 92.28°, 96.99°, and 90.13°. The mean value for the change in Fe-N bonds is $\Delta r_{Fe \to N} \approx 0.154$ Å[12], [13].

1.1.2 Thermodynamics of spin crossover in $[\mathbf{Fe\{H_2B\,(pz)_2\}_2\,(bipy)}]$

The spin state transition in $[Fe\{H_2B\,(pz)_2\}_2\,(bipy)]$ is an abrupt one, and may be considered discontinuous. It can therefore be spoken of in terms of critical transition temperature $T_{1/2}$, at which point the fraction of molecules in the HS state is $\gamma_{HS} = 0.50$. Considering that the Gibbs free energy is expressed as

$$\Delta G = \Delta H - T\Delta S \tag{1.2}$$

for equal populations of HS and LS, the Gibbs energy is now

$$\Delta G = G_{HS} - G_{LS} = 0 \tag{1.3}$$

and noting

$$\Delta H = H_{HS} - H_{LS} \tag{1.4}$$

$$\Delta S = S_{HS} - S_{LS} \tag{1.5}$$

we have an entropy driven expression for the critical temperature:

$$T_{1/2} = \frac{\Delta H}{\Delta S}. \tag{1.6}$$

The $T\Delta S$ term in eq. 1.2 will dominate, making the state with the most entropy the stable one. The change in entropy may be further divided into two contributing factors, namely ΔS_{el} and ΔS_{vib}, or the ratio of degeneracy between high and low states($\Delta S_{\mathrm{el}} = Nk_B \ln \frac{g_{HS}}{g_{LS}}$), and the vibrational entropy respectively. For Fe(II) octahedral compounds, both ΔS_{el} and ΔS_{vib} are positive. In order for a spin transition to be possible, the LS potential well must be lower than the HS potential[14], as shown in Figure 1.3.

Generally speaking, the change from a LS to HS state in octahedral transition metal spin crossover compounds may occur in a continuous manner, or may be abrupt. In some species, the thin films exhibit a much more gradual shift than the bulk. For $[Fe\{H_2B\,(pz)_2\}_2\,(bipy)]$ the transition is abrupt, and the thin film exhibits a sharp transition in a nearly identical way

as in the bulk [15]. Figure 1.4 shows data taken by Palamarciuc et al looking at the magnetic susceptibility times temperature as a function of temperature of $[Fe\{H_2B\,(pz)_2\}_2\,(bipy)]$ and sister Fe(II) coordination compound $[Fe\{H_2B\,(pz)_2\}_2\,(phen)]$ (phen = 9,10-phenanthroline).

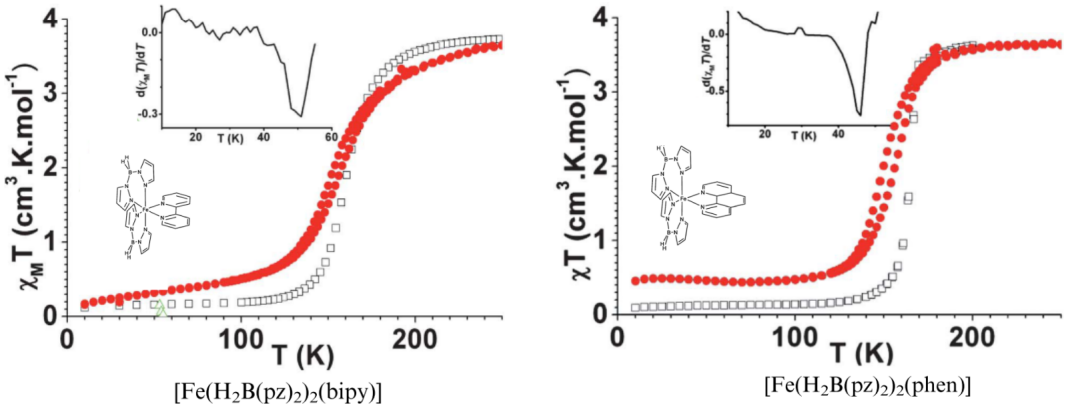

Figure 1.4. The abrupt nature of the transition from HS to LS in $[Fe\{H_2B\,(pz)_2\}_2\,(bipy)]$: 355nm thin film at 1T (red filled circles), and bulk at 1T (black squares). The transitions are very similar.[15]

The abrupt spin state transition of $[Fe\{H_2B\,(pz)_2\}_2\,(bipy)]$ makes it a good candidate for studies which seek to exploit the switchable nature of SCO molecules and their propensity for device applications. Work by Palamarciuc et al, and previous works by Real et al and Bouseesskou et al, show that $[Fe\{H_2B\,(pz)_2\}_2\,(bipy)]$ is sublimable, displays cooperativity and spin crossover, and maintains the abrupt nature of its SCO transition after sublimation in order to form thin films [15]–[18]. Note that these studies focus on global methods to change the thermodynamic surroundings of the sample, as opposed to stimuli which are scalable and capable of addressing local regions or single molecules. More discussion on this is in *Chapter 2. Background and Theoretical* of this report. For now, let us consider a platform for using the electric field from a highly polarized environment, such as a ferroelectric substrate, to induce the SCO.

1.1.3 A dynamic substrate: ferroelectric polyvinylidene flouride

The quintessential ferroelectric polymer polyvinylidene flouride (PVDF), and its common co-polymers, is among the most well-studied of the non-Perovskite organic ferroelectrics. It

exhibits many properties which make it desirable for device and laboratory applications, including; ease of fabrication, near-monolayer control of thickness, mechanical conformability and flexibility, and very stable reversible polarization [19]–[21]. Since PVDF will respond to force, pressure, strain, vibration and temperature, it has already found use in next-generation sensors [22].

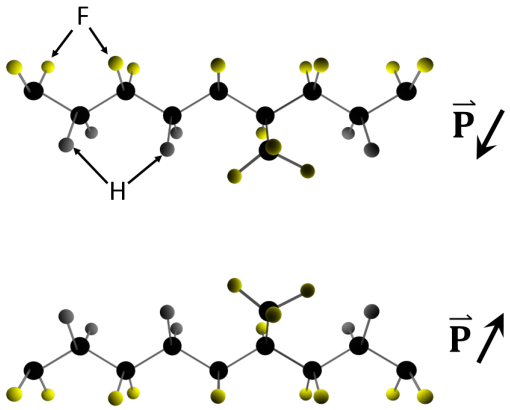

Figure 1.5. The ferroelectric β-phase crystalline conformation of Polyvinylidene Fluoride (PVDF) consists of a carbon backbone with a transverse dipole terminating in fluorine on one end and hydrogen on the other. The co-polymer Hexafluoropropylene (HFP) provides an electrostatic interaction which keeps the polymer chains ordered, promoting the β-phase. Image courtesy of Ashley Dale.

PVDF belongs to the class of ferroelectrics known as order-disorder ferroelectrics. This group is typified by a transition from randomly distributed dipoles, to ordered dipoles resulting in a spontaneous polarization [22], [23]. This is a first order thermodynamic phase transition, and PVDF readily displays a hysteretic response to an external coercive field.

Structurally, the polymer chain consists of a repeated $-CH_2CF_2$ monomer, and it may take a trans (F) or gauche (G) conformation along its axis [24], [25]. The four crystal phases of PVDF, known as the α (TGTG'), β (TTTT) as in Figure 1.5, γ (T_3GT_3G), and δ (a mirror of the α phase) phases exhibit differing properties [26]. The α and δ phases dipole moment is cancelled due to the orientation of the flourine ions. Both the β and γ phase of PVDF are electro-active, however the γ phase exhibits a rather weak dipole moment considering its T_3GT_3G conformation [27]. It is the TTTT orientation of the he β phase crystal configuration

of the molecule which exhibits a robust polarization with a broad thermal stability range. More information about the crystalline structure of PVDF and its co-polymers is available in the references.

Achieving the ordered β phase in PVDF may be done in a variety of ways including (but not limited to!) stretching, thermal annealing, by the addition of metallic particles, carbon nanorods, or other nucleation inducing materials, and the addition of co-polymers[28]. Since the TTTT phase avoids the steric hindrance present in the other phases, it is energetically favored, and therefore annealing of the material will allow it to relax into the β phase. Thermal annealing is an excellent route towards a thorough β-phase crystalline ordering and is carried out at reasonable temperatures and time scales. Previous works in our lab have shown that optimal annealing temperature for PVDF is around 130° C [29]. While this is most certainly a preferred method, it is not always possible to use as it may damage other layers of a proposed device if they are sensitive to temperatures at or around 130°. This issue will be encountered later in this study.

The addition of a co-polymer to PVDF also helps to induce β phase. The most famous of these, poly(vinylidene fluoride-trifluoroethylene) (PVDF-TrFE), has a considerable body of research work available. The introduction of the trifluoroethylene monomer into the polymer chain increases the distance between monomer bonds in the chain, thus lowering the energy barrier for rotation, and has also shown pinning behavior, facilitating the rotation of the fluorine ions to achieve a TTTT conformation [30]–[32]. Polyvinylidene Flouride Hexafluoropropylene (PVDF-HFP) is another such copolymer, and is the copolymer used in this study. To our knowledge, this is the first instance of using this particular co-polymer to induce a spin state transition in a molecular thin film. Much less is known about it, although it is not a new material [27], [33]–[36]. Figure 1.5 shows a representative polymer chain of β phase PVDF-HFP. Reports show that the annealing temperature of 120°C for PVDF-HFP is slighlty less than that of pure PVDF [37].

1.2 Charge transport in spin crossover molecules

Insight into the mechanisms responsible for the observed change in dielectric properties, and hence conductance switching in Fe(II) SCO molecules, is still very much an open

question. The modelling of SCO molecules comes with an inherent difficulty, in that the defining parameter of a spin crossover system is its transition temperature $T_{1/2}$, which is a thermodynamic parameter. In other words, it does not make sense to look at the $T_{1/2}$ of a single molecule. The use of density functional theory (DFT) to predict and describe energy level differences between suborbitals is filled with challenges, often giving over-estimations for both the LS or HS state energy level, depending on the specific functional used. Progress has been made however, and the reader is directed to references [38]–[42] for more detail on DFT methods with Fe(II) SCO systems.

From the experimental perspective, conductance switching has been characterized for a variety of Fe(II) compounds in various thicknesses and configurations. A study which successfully incorporates both DFT theoretical predictions with IV measurements of a single SCO molecule was performed by Aravena et al., the assertion here is that the β electron in the S=2 t_{2g}^4 e_g^2, or the unpaired electron in the HS state, is shifted close to the Fermi level [43]. Further, they suggest that the HS molecule acts as a spin filter due to the higher admission of the unpaired β electrons into the conduction band. This latter part is interesting indeed, and certainly worthy of further study, perhaps with spin-polarized scanning tunneling microscopy as a probe. A word of caution concerning this study. Single molecule studies are notoriously difficult, and present a range of issues not the least of which, in the case of SCO molecules, is the interaction of the metallic electrode with the lone molecule [7], [43]–[46]. It is difficult to accurately assess the contribution of the surface chemistry of the electrode to the distortion of the Fe(II) frontier orbitals.

A more general approach is given by Baadji and Sanuito using a DFT-combined-with-non-equilibrium-Green's-function method for quantum transport [47]. Here it is shown that certain electronic configurations of the frontier orbitals, namely the e_g and t_{2g} splitting, lead to changes in the energy gap between the highest occupied molecular orbital (HOMO) and the lowest unoccupied molecular orbital (LUMO). This HOMO-LUMO energy gap produces large changes in the observed IV curves of Fe(II) complexes. Simply put, the combination of the HOMO-LUMO splitting and the absence of pairing energy on the electrons in the HS state promote and easier jump into the conduction band.

2. BACKGROUND AND THEORETICAL

2.1 Background and previous works

The first observations of the spin crossover state transition were in an Fe(III) complex. and was conducted in the 1930's by Cambi et al. recorded and published "unusual" magnetic properties in ferric dimethyl dithiocarbamate, or iron tris(dimethyldithiocarbamate) under amine substitution [48]. Very close to the same time of these experiments, Hans Bethe had fully developed crystal field theory [49], capable of describing the energetic splitting of the d orbital in a central ion surrounded by a ligand field. By 1967 we see the first published report of spin crossover in Fe(II) complexes $[Fe(phen)_2(NCS)_2]$ and $[Fe(phen)_2(NCSe)_2]$, which were characterized by using Mössbauer spectroscopy [50].

Clearly, the exploration of spin crossover phenomena is not a new field, but as of the last 5-7 years it is an accelerated one. The research surrounding the phenomenon lies at the intersection of synthetic chemistry, materials and electrical engineering, and solid state physics. An interdisciplinary quest of this type can yield many beneficial findings across science and technology as a whole.

Recently, much attention has been given to understanding the mechanism of spin crossover as it relates to the molecule's local environment. Research has moved away from global mechanisms such as temperature and light and refocused on electric field. Justifiably so, for in order to create a useful device based on coordination compounds, and utilize their full molecular based potential, local control is vital. Some current questions that are being asked (and answered) are: What happens at the interface of a SCO thin film and a conductor, or ferromagentic thin film? Does the molecule live in a mostly anisotropic or isotropic environment? Can this local environment be controlled externally? What is the energy cost associated with externally controlled switching?

In 2014, after work which characterized light induced spin state switching[51], Peter Dowben's group at the University of Nebraska showed that the spin state of $[Fe\{H_2B(pz)_2\}_2(bipy)]$ could be locked into a mostly LS state configuration, above it's transition temperature, by controlling the polarization of it's ferroelectric polyvinlyidene flouride-trifluoroethylene (PVDF-TrFE) substrate [52]. This work was inspired by previous

works carried out by the group which looked at adsorbate/substrate interactions [53]–[55], showing that significant changes in conformation, dipole moment, and energy level alignment can occur.

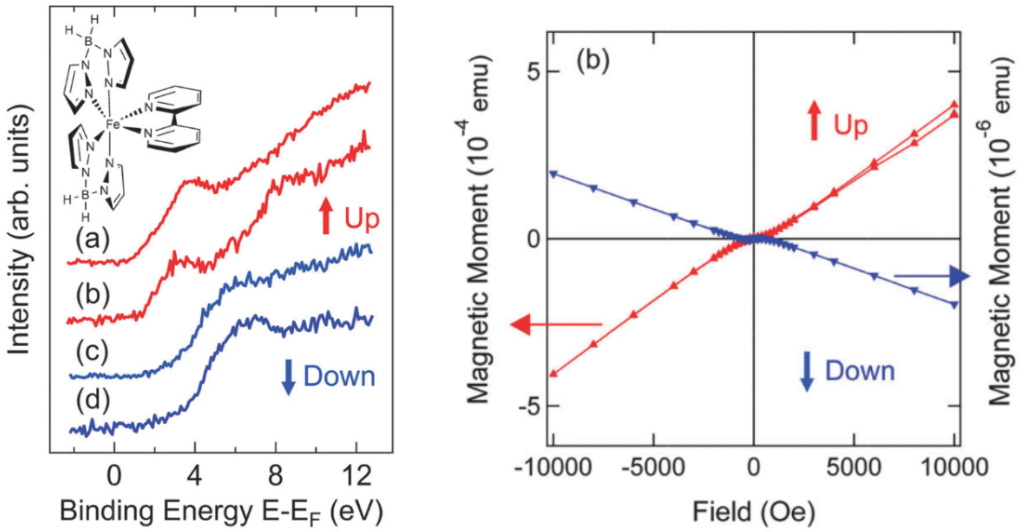

Figure 2.1. On the left, inverse photoemission spectroscopy shows a shift in electronic configuration for $[Fe\{H_2B\,(pz)_2\}_2\,(bipy)]$ thin films deposited on a ferroelectric PVDF-TrFE substrate. The spin state of the adsorbate is coupled to the polarization of the substrate. On the right, SQUID magnetometer data showing the paramagnetic HS state and diamagnetic LS state [52].

In the study, thermally deposited 10-20nm thick $[Fe\{H_2B\,(pz)_2\}_2\,(bipy)]$ thin films on a 3nm poled ferroelectric PVDF-TrFE substrate, which was deposited on Al_2O_3 using the Langmuir Blodgett method were made. Inverse photoemission spectroscopy was used to characterize electronic structure, and show the subsequent change in orbital population, and a SQUID magnetometer was used to characterize the diamagnetic low spin and paramagnetic high spin magnetic states. This data is shown in Figure 2.1.

Interaction of very thin layers of the SCO molecule $[Fe\{H_2B\,(pz)_2\}_2\,(bipy)]$ with a Au(111) substrate [17] was thoroughly characterized in 2016 by scanning tunneling microscopy, X-Ray absorption spectroscopy, and X-Ray photoemission. This study showed that very thin samples of a few monolayers, or roughly 2D films, would be irreversibly locked into a mixed, mostly LS state, even above the transition temperature, when deposited on a metallic substrate. This locking did not occur immediately upon adsorption, but once

the temperature had been lowered down past the transition point. The locking phenomena is attributed to a locking of the conformation of the molecule after it has undergone the transition to the LS state. Previous studies by other groups on different SCO molecules also give compelling proof that the behavior of the spin state transition in very thin molecular SCO thin films and single molecules can be influenced by interactions with the substrate [44], [56].

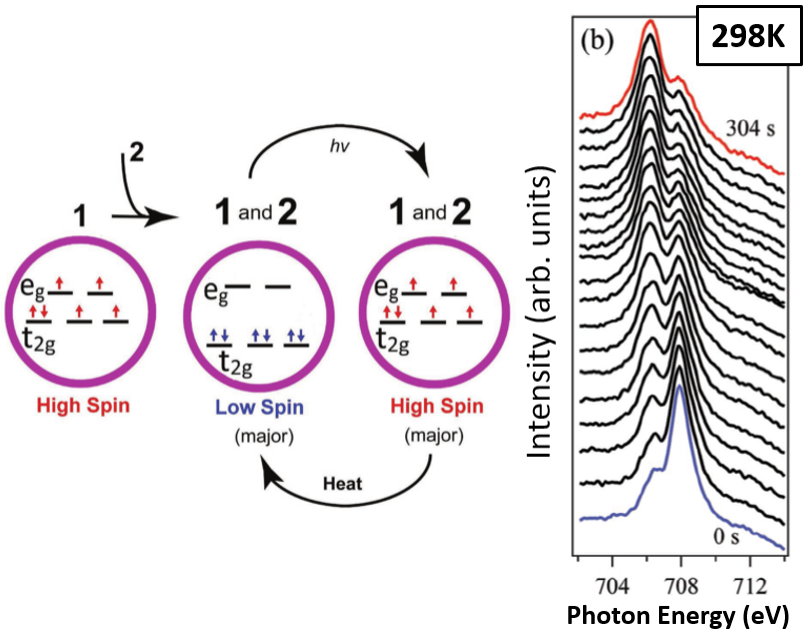

Figure 2.2. When in a highly polar environment, the spin state of $[Fe\{H_2B(pz)_2\}_2(bipy)]$ stays locked in a mostly LS state, even up to room temperature. Photoexcitation by X-Ray fluence, as shown in the XAS data above[57], will push the molecule into the mostly HS state, and then slightly warming the molecule by 10-20K will let it relax back into the LS state.

To further probe the interaction between the molecule and a polarized environment, $[Fe\{H_2B(pz)_2\}_2(bipy)]$ was put into solution with the strongly polar zwitterion *p*-benzoquinonemonoimine $C_6H_2(...NH_2)_2(...O)_2$. It is observed that this will lock the spin state of the molecule into the mostly LS configuration up to room temperature, which is well above the transition point [57]. Then photoexcitation can be used to transition the molecule into the HS state, as clearly seen in Figure 2.2. Slight warming of the molecule by 10-20K will allow it to relax back down into the mostly LS state. Also, this same study showed behavior of very thin films of $[Fe\{H_2B(pz)_2\}_2(bipy)]$ deposited on the dielectric substrates

SiO_2 and Al_2O_2 to be very similar to that observed previously (the 2016 study from above) by films deposited on Au(111), in that the spin state will be locked into the LS state upon cooling and re-warming.

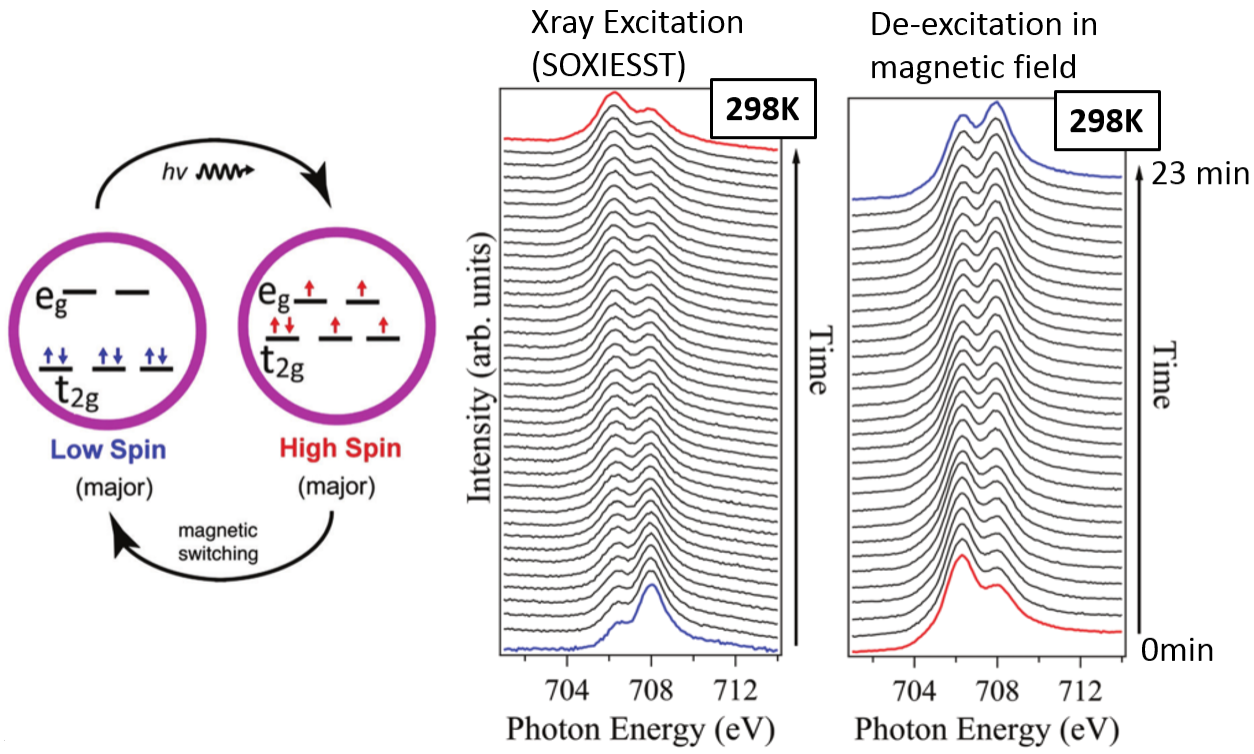

Figure 2.3. The XAS data on the left shows a thin film of $[Fe\{H_2B(pz)_2\}_2(bipy)]$ deposited on a ferromagnetic substrate of $NiCo_2O_4$ locked into a LS state at room temperature and then excited to a mixed, mostly HS state. The XAS data on the right shows the de-excitation of the molecule back to a mostly LS state at room temperature by the interaction of the sample with an oscillating magnetic field of ± 1[58].

By depositing a thin film of $[Fe\{H_2B(pz)_2\}_2(bipy)]$ onto a ferromagnetic $NiCo_2O_4$ substrate, magnetic coupling effects were studied in 2018 by Zhang and Dowben [58]. This study showed a locking of the LS state at room temperature, excitation into HS state by X-Ray fluence, and then relaxation back into the LS state at room temperature by exposing the sample to an oscillating magnetic field. The XAS data in Figure 2.3 shows that a 23 minute exposure to a ± 1T oscillating magnetic field with a period of 1 minute, will relax the molecule back into a LS state even after photoexcitation into a mixed, mostly HS state.

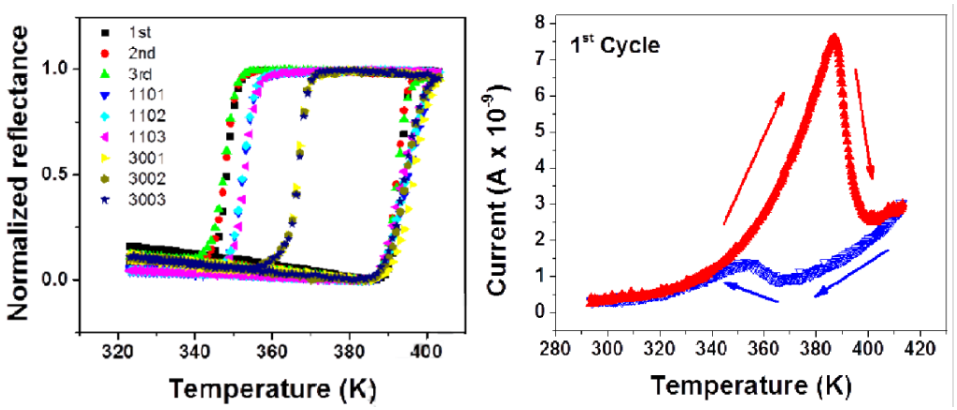

Figure 2.4. This data shows current switching and spin state transition in a spin crossover based device. Micro-scaled rods of an Fe(II) coordination complex. The spin state of the material, shown if the left graph as monitored by optical spectroscopy reflectance measurements, is changed as a function of temperature. Thermal cycling was done over 3000 times and the material retained its spin crossover properties. The conductance, measured by positioning the micro-rods across gold electrodes is then shown to change at the transition temperature on the right. It is shown to be robust up to 20 times [59].

Numerous studies have shown viable, high-yield devices based on molecular materials [60]. Most devices based on the spin crossover phenomena utilize light and temperature and are therefore unable to exploit the potential for inherent scalability. One work of note, conducted by Azzedine Bousseksou's group at the Universite' de Toulouse includes the switching of spin crossover micro-rods laying across gold electrodes by thermal cycling. Spin crossover behavior, monitored by reflectance readings with a Raman spectrometer, was stable after over 3000 cycles of the spin state transition. Current measurements were also taken showing a conductance switching coinciding with the spin state change at up to 20 cycles.

In the next section, the theoretical underpinnings for the basic spin state transition in an octahedral coordination complex will be presented. We will see a partial lifting of degeneracy in the frontier orbital energetics of the central metallic ion which results in distinct, energetically stable spin state configurations.

2.2 The theory for the energy splitting of the d orbital in an octahedral coordination compound

Starting with a spherical potential and the Hamiltonian for the familiar Hydrogenic atom,

$$\hat{\mathcal{H}}_{\mathrm{ij}} = -\left(\frac{\hbar^2}{2m}\right)\nabla^2 - Z_{eff}\frac{\mathrm{e}^2}{r}, \tag{2.1}$$

we arrive at the following d orbital wavefunctions:

$$d_{z^2} = |0\rangle \tag{2.2}$$

$$d_{yz} = \frac{-\mathrm{i}}{\sqrt{2}}\left[|1\rangle + |-1\rangle\right] \tag{2.3}$$

$$d_{xz} = \frac{1}{\sqrt{2}}\left[|1\rangle - |-1\rangle\right] \tag{2.4}$$

$$d_{xy} = \frac{-\mathrm{i}}{\sqrt{2}}\left[|2\rangle - |-2\rangle\right] \tag{2.5}$$

$$d_{x^2-y^2} = \frac{1}{\sqrt{2}}\left[|2\rangle + |-2\rangle\right]. \tag{2.6}$$

Now consider 6 point charges in an octahedral geometry around the central "nucleus" or ion in this case. This will be the basis for our new, perturbed Hamiltonian. From degenerate time independent perturbation theory

$$\hat{\mathcal{H}}_{\circ}\,|\psi_{\mathrm{i}}\rangle = E_{\circ}\,|\psi_{\mathrm{i}}\rangle \tag{2.7}$$

$$\implies \left(\hat{\mathcal{H}}_{\circ} + \hat{\mathcal{H}}\right)|\psi_{\mathrm{j}}\rangle = E_{\mathrm{j}}\,|\psi_{\mathrm{j}}\rangle\,. \tag{2.8}$$

We modify the Hamiltonian by first creating a field consisting of 6 point charges around the ion, which works out like an electrostatics problem.

$$V_{(x,y,z)} = \sum_{\mathrm{i}=1}^{6} Z\frac{\mathrm{e}^2}{r_{\mathrm{ij}}} \tag{2.9}$$

Employing spherical harmonics, it can be shown that the contribution from a potential due to one point charge is

$$V_1 = \frac{Z\mathrm{e}^2}{a}\sum_{l=o}^{4}\left(\frac{r}{a}\right)^l P_l\left(\cos\theta\right) \tag{2.10}$$

$$V_1 = \frac{Z\mathrm{e}^2}{a}\Bigg[1+\left(\frac{r}{a}\right)P_1\left(cos\theta\right)+\left(\frac{r}{a}\right)^2 P_2\left(\cos\theta\right) + \left(\frac{r}{a}\right)^3 P_3\left(\cos\theta\right)+\left(\frac{r}{a}\right)^4 P_4\left(\cos\theta\right)\Bigg]. \tag{2.11}$$

Rotating by $\boldsymbol{\pi}$ and adding $V_1 + V_2$ (note that $\cos\left(\theta+\boldsymbol{\pi}\right) = -\cos\left(\theta\right)$),

$$V_1 + V_2 = \frac{2Z\mathrm{e}^2}{a}\left[1+\left(\frac{r}{a}\right)^2 P_2\left(\cos\theta\right)+\left(\frac{r}{a}\right)^4 P_4\left(\cos\theta\right)\right]. \tag{2.12}$$

Substituting the appropriate Legendre polynomials and making the change of variables $\cos\theta = z/r$,

$$V_1 + V_2 = \frac{2Z\mathrm{e}^2}{a}\left[1+\frac{1}{2}\left(\frac{r}{a}\right)^2\left(\frac{3Z^2}{r^2}-1\right)+\frac{1}{8}\left(\frac{r}{a}\right)^4\left(\frac{35z^4}{r^4}-\frac{30z^2}{r^2}+3\right)\right]. \tag{2.13}$$

This method can be applied to $V_3 + V_4$ and $V_5 + V_6$ to create the complete potential

$$V = 6\frac{Z\mathrm{e}^2}{a}+\frac{35Z\mathrm{e}^2}{4a^5}\left(x^4+y^4+z^4-\frac{3}{5}r^4\right) \tag{2.14}$$

$$= 6\frac{Z\mathrm{e}^2}{a}+D\left(x^4+y^4+z^4-\frac{3}{5}r^4\right). \tag{2.15}$$

The parameter D is defined as

$$D = \frac{35Z\mathrm{e}^2}{4a^5}. \tag{2.16}$$

It is now necessary to calculate the values for the matrix elements which describe the energy of the perturbed Hamiltonian. First order energy is given by

$$\langle\psi^*|\,\hat{\mathcal{H}}\,|\psi\rangle\,. \tag{2.17}$$

The nature of the five wavefunctions for the d orbital is such that the system is five-fold degenerate, allowing us to write

$$\langle m_l | \hat{\mathcal{H}} | m_l \rangle, \tag{2.18}$$

$$\hat{\mathcal{H}} = V(r) V(\theta, \phi) \implies \langle R_{nl} | V(r) | R_{nl} \rangle \langle lm | V(\theta, \phi) | lm \rangle \tag{2.19}$$

$$= \int_0^\infty R_{nl}(r) V(r) R_{nl}(r) r^2 dr \int_0^\pi \int_0^{2\pi} \Theta_{lm}(\theta) \Phi(\phi)$$

$$V(\theta, \phi) \Theta_{lm}(\theta) \Phi(\phi_m) \sin\theta d\theta d\phi. \tag{2.20}$$

The wavefunctions of the d orbital have the form

$$\Psi_{nlm} = R_{nl}(r) \Theta_{lm}(\theta) \Phi_m(\phi), \tag{2.21}$$

and we will need elements

$$\langle m | D \left(x^4 + y^4 + z^4 \right) | m \rangle .$$

From

$$x^4 + y^4 + z^4 = r^4 \sin^4\theta \left(\sin^4\phi + \cos^4\phi \right) + r^4 \cos^4\theta$$

evaluating the Φ terms:

$$\langle \Phi_m | \sin^4\phi + \cos^4\phi | \Phi_m \rangle = \int_0^{2\pi} \mathrm{e}^{\mathrm{i}m\phi} \left(\sin^4\phi + \cos^4\phi \right) \mathrm{e}^{-\mathrm{i}m\phi} d\phi \tag{2.22}$$

$$= \tfrac{1}{8} \int \mathrm{e}^{\mathrm{i}m\phi} \left(\mathrm{e}^{4\mathrm{i}\phi} + \mathrm{e}^{-4\mathrm{i}\phi} + 6 \right) \mathrm{e}^{-\mathrm{i}m\phi} d\phi \tag{2.23}$$

$$= \begin{cases} \frac{1}{8} r^4 \sin^4\theta \text{ for } m = m \pm 4 \\ \frac{3}{4} r^4 \sin^4\theta \text{ for } m = m \\ 0 \text{ else.} \end{cases} \tag{2.24}$$

There are now seven non-zero values for the secular determinant. In matrix form we have;

$$\begin{bmatrix} \langle 2|\,\hat{\mathcal{H}}\,|2\rangle & 0 & 0 & 0 & \langle 2|\,\hat{\mathcal{H}}\,|-2\rangle \\ 0 & \langle 1|\,\hat{\mathcal{H}}\,|1\rangle & 0 & 0 & 0 \\ 0 & 0 & \langle 0|\,\hat{\mathcal{H}}\,|0\rangle & 0 & 0 \\ 0 & 0 & 0 & \langle -1|\,\hat{\mathcal{H}}\,|-1\rangle & 0 \\ \langle -2|\,\hat{\mathcal{H}}\,|2\rangle & 0 & 0 & 0 & \langle -2|\,\hat{\mathcal{H}}\,|-2\rangle \end{bmatrix} = 0$$

$$\text{where } \hat{\mathcal{H}} = D(x^4 + y^4 + z^4).$$

Next we can tackle the Θ_{lm} terms. Note that for Fe we are dealing with d orbitals therefore $l = 2$ always, and m_l will be written as m for simplicity. Although they are a little more complicated, there will only be 7 to consider. The form of the integral is

$$D\int_0^{\pi} \Theta_{lm}\,\langle\Phi_m|\,(x^4 + y^4 + z^4)\,|\Phi_m\rangle\,\Theta_{lm}\sin\theta\,d\theta \tag{2.25}$$

considering $m = m$ and $z = r\cos\theta$,

$$r^4\,\langle\Theta_{20}|\left(\tfrac{3}{4}\sin^4\theta + \cos^4\theta\right)|\Theta_{20}\rangle \\ = \tfrac{5}{8}r^4\int_0^{\pi}(3\cos^2\theta - 1)^2(\tfrac{3}{4}\sin^4\theta + cos^4\theta)sin\theta d\theta$$

All 7 Θ integrals are thus worked out to be

$$\langle 0|\,(x^4 + y^4 + z^4)\,|0\rangle = \tfrac{5}{7}r^4 \tag{2.26}$$

$$\langle 1|\,(x^4 + y^4 + z^4)\,|1\rangle = \langle -1|\,(x^4 + y^4 + z^4)\,|-1\rangle = \tfrac{11}{21}r^4 \tag{2.27}$$

$$\langle 2|\,(x^4 + y^4 + z^4)\,|2\rangle = \langle -2|\,(x^4 + y^4 + z^4)\,|-2\rangle = \tfrac{13}{21}r^4 \tag{2.28}$$

$$\langle 2|\,(x^4 + y^4 + z^4)\,|-2\rangle = \langle -2|\,(x^4 + y^4 + z^4)\,|2\rangle = \tfrac{73}{105}r^4 \tag{2.29}$$

Next, the radial component must be dealt with. By perturbing the original Hamiltonian, we have a system that is different from a simple Hydrogen-like configuration, and is therefore

not practical to solve. It becomes necessary to parameterize the integral. The integral can however be parameterized. Beginning with the integral

$$\langle\psi(0)|\, V\, |\psi(0)\rangle \equiv \langle\psi(0)|\, D(x^4+y^4+z^4-\tfrac{3}{5}r^4)\, |\psi(0)\rangle \tag{2.30}$$

$$=\tfrac{5}{7}D\int_0^\infty R_{nl}^2 r^6 dr - \tfrac{3}{5}D\int_0^\infty R_{nl}^2 r^6 dr \tag{2.31}$$

$$=\tfrac{12}{105}D\int_0^\infty R_{nl}^2 r^6 dr = 6Dq \tag{2.32}$$

where

$$q = \tfrac{2}{105}\int_0^\infty R_{nl}^2 r^6 dr = \tfrac{2}{105} r_{avg}^4 \tag{2.33}$$

similarly

$$\langle\psi(1)|\, V\, |\psi(1)\rangle \equiv \langle\psi(-1)|\, V\, |\psi(-1)\rangle = -4Dq \tag{2.34}$$

$$\langle\psi(2)|\, V\, |\psi(2)\rangle \equiv \langle\psi(-2)|\, V\, |\psi(-2)\rangle = Dq \tag{2.35}$$

$$\langle\psi(-2)|\, V\, |\psi(2)\rangle \equiv \langle\psi(2)|\, V\, |\psi(-2)\rangle = 5Dq \tag{2.36}$$

the perturbed energy secular determinant is

$$\begin{bmatrix} Dq-E & 0 & 0 & 0 & 5Dq \\ 0 & -4Dq-E & 0 & 0 & 0 \\ 0 & 0 & 6Dq-E & 0 & 0 \\ 0 & 0 & 0 & -4Dq-E & 0 \\ 5Dq & 0 & 0 & 0 & Dq-E \end{bmatrix} = 0.$$

The energies for our perturbed system are

$E_1 = -4Dq$ with 3-fold degeneracy

and

$E_2 = 6Dq$ with 2-fold degeneracy.

These energies correspond to the wavefunctions:

$$-4Dq \begin{cases} d_{yz} & = \frac{-\mathrm{i}}{\sqrt{2}} \left[|1\rangle + |-1\rangle \right] \\ d_{xz} & = \frac{1}{\sqrt{2}} \left[|1\rangle - |-1\rangle \right] \\ d_{xy} & = \frac{-\mathrm{i}}{\sqrt{2}} \left[|2\rangle - |-2\rangle \right], \end{cases}$$

which we label the e_g orbital and

$$6Dq \begin{cases} d_{z^2} = |0\rangle \\ d_{x^2-y^2} = \frac{1}{\sqrt{2}} \left[|2\rangle + |-2\rangle \right], \end{cases}$$

which we label the t_{2g} orbital.

It is now clear the there is a partial breaking of the degeneracy of the frontier orbital of our central transition metal ion, in an octahedral geometry, and that it gives rise to a splitting of the orbital [61], [62].

2.2.1 Electric field control of the spin state in $[\mathbf{Fe\{H_2B\,(pz)_2\}_2\,(bipy)}]$ thin films

The main focus of this study is the voltage control of the spin state, and thus voltage control of the conductivity of $[Fe\{H_2B\,(pz)_2\}_2\,(bipy)]$. This is accomplished by using a multilayered thin film sample, consisting of the SCO material interfaced to a ferroelectric polymer. External control of the ferroelectric's polarization will give control of the local energetic environment of the SCO molecule, namely a very large electric field, at the interface.

In order to examine this theoretically, and build a suitable model for the observed phenomena, the addition of an extra term in the perturbing Hamiltonian to account for the electric field is proposed. This would at least give a general outline for the energetic change of the system upon polarization reversal, and it's effect upon the spitting of the e_g and t_{2g} orbitals of the central Fe ion.

Adding the electric field term to the perturbing potential (2.23),

$$V = 6\frac{Z\mathrm{e}^2}{a} + D\left(x^4 + y^4 + z^4 - \tfrac{3}{5}r^4\right) - Er\cos\theta. \tag{2.37}$$

Since the electric field term is not ϕ dependent, we would then work through all the θ terms, for example the $\Theta_{21}, \Theta_{2-1}$ terms are calculated following the form of (2.36).

Further investigation of the paring energy of the electrons in the frontier orbitals of the Fe may also be in order. This would require the calculation of the exact spin pairing energies [10] for $[Fe\{H_2B\,(pz)_2\}_2\,(bipy)]$ to get an accurate value for $10Dq$. *Ab initio* molecular modeling of the phenomena, namely the coupling of the energetic splitting to the electric field of the ferroelectric, could also provide an insightful picture, and help with the future design of spintronic devices utilizing the same or similar constituent parts.

2.3 Model to examine the energy difference of the spin state transition

As has been established in previous studies, the activation energies for spin state transition may be perturbed by a polar interface. An observed difference in $T_{1/2}$, or more generally, $\gamma_{LS/HS}$ of $[Fe\{H_2B\,(pz)_2\}_2\,(bipy)]$ is useful in determining the energy needed for switching. Detailed experimental data will be presented in *Chapter 3 : Data and Discussion* of this thesis. In order to set the stage for that analysis, an overview of the theoretical model for the examination of the activation energy difference will be presented here.

Considering the evolution of the density of states for the t_{2g} and e_g orbitals as a function of change in temperature, in the different electric field orientation as produced by the polarized ferroelectric layer, the energetics involved in the field induced transition between the HS and LS states may be examined [63]. The phase transition between HS and LS states of SCO molecules can be simulated by an Ising-like model, where the two discrete values correspond to the HS and LS states, respectively [64]–[68]. A typical Ising Hamiltonian for a two-level system is

$$\hat{\mathcal{H}}_{ij} = -J \sum_{i,j} S(i,j)S(i \pm 1, j \pm 1) + \frac{\Delta}{2} \sum_{i,j} S_{i,j} \tag{2.38}$$

This basic Ising Hamiltonian can be modified to describe a spin crossover system (which is essentially a two-level system) by taking into account the activation energy for transitioning between the HS and LS states, and the contribution due to degenerate states.

We can take the eigenvalues of the operators $S_{\mathrm{i,j}}$ to be 1 and -1 for HS and LS respectively. J is the interaction between molecules, and $\Delta_\circ$ represents the energy difference between the HS and LS state. With g as the degeneracy ratio, i.e. the ratio of degenerate HS to degenerate LS states,

$$g = \frac{g_{HS}}{g_{LS}}, \tag{2.39}$$

the contribution of entropy is

$$k_B \ln g. \tag{2.40}$$

A refined Hamiltonian, which will be used to probe the energetics of switching the ferroelectric/spin crossover system, takes the form

$$\hat{\mathcal{H}}_{\mathrm{ij}} = -J \sum_{\mathrm{i,j}} S(\mathrm{i,j}) S(\mathrm{i} \pm 1, \mathrm{j} \pm 1) + \left(\frac{\Delta_\circ}{2} - \frac{k_B T}{2} \ln g \right) \sum_{\mathrm{i,j}} S_{\mathrm{i,j}}. \tag{2.41}$$

3. EXPERIMENTAL TECHNIQUES AND SAMPLE PREPARATION

3.1 X-ray diffraction

The primary mechanism for the creation of an X-ray Diffraction (XRD) spectrum is the constructive interference created by the elastic scattering of light from the periodic arrays of ions in a crystal lattice. Considering that a reasonable inter-ionic distance in a perfect array would be on the scale of angstroms

$$\frac{hc}{\lambda} = \frac{(4.136x10^{-15}\text{eV}\cdot s)(2.997x10^{8}\frac{m}{s})}{0.275x10^{-9}m} \approx 4.5x10^{3}\text{eV}$$

puts the energy of an ideal probe squarely in the x-Ray region of the electromagnetic spectrum.

There are two equivalent formalisms for describing x-ray scattering from a periodic array. The Bragg criterion rests on two assumptions, namely that the light is specularly reflected from planes created by the perfect periodic arrays of the crystal lattice, and that these rays, reflected from successive planes, will constructively interfere [69] resulting in the familiar equation

$$n\lambda = 2d\sin\theta. \tag{3.1}$$

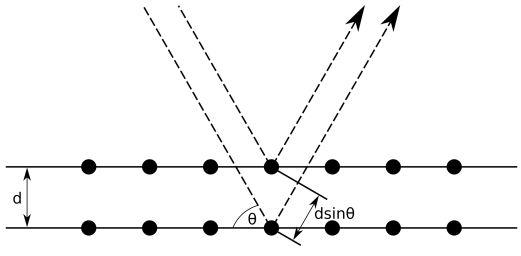

Figure 3.1. Geometric representation of the Bragg condition resulting in the constructive interference of light scattered from two successive planes spaced apart by distance d. Image by Furiouslettuce - Public Domain, https://commons. wikimedia.org/w/index.php?curid=6487785

In contrast to the Bragg formalism, the Laue criterion does not presupposed specular reflection nor specific ordering of crystal planes as conditions for constructive interference. Each ion in the lattice acts as a scattering center emitting wavelets that interfere according to Huygen's principle. The incoming plane wave and corresponding wavevector are

$$e^{i\mathbf{k}\cdot\mathbf{r}} = \cos\mathbf{k}\cdot\mathbf{r} + i\sin\mathbf{k}\cdot\mathbf{r} \tag{3.2}$$

$$\mathbf{k} = \frac{2\pi}{\lambda}\hat{n} \tag{3.3}$$

with the new scattered wave having wavevector

$$\mathbf{k} = \frac{2\pi}{\lambda}\hat{n}$$

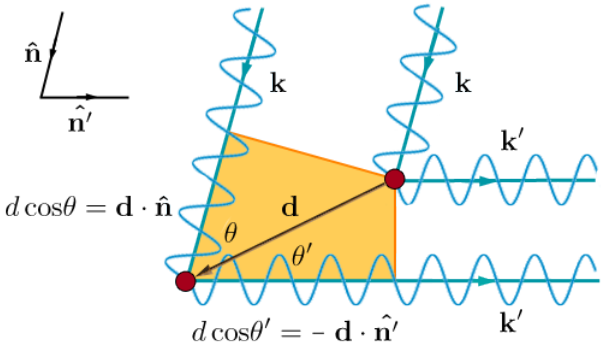

Figure 3.2. Geometric representation of the Laue condition resulting in the constructive interference of light scattered from two scattering sites in a lattice spaced apart by distance **d**. Image by By Shawmbo - Own work, CC BY-SA 3.0, https://commons.wikimedia.org/w/index.php?curid=8093469

Constructive interference is then given by

$$|\mathbf{d}|\cos\theta + |\mathbf{d}|\cos\theta = \mathbf{d}\cdot(\hat{\mathbf{n}} - \hat{\mathbf{n}}) = m\theta \tag{3.4}$$

Since the direction and intensity of the diffraction spectra obtained depend upon the spacing of atoms in the crystal lattice, and thus attributes of the unit cell, specific infor-

mation about composition, crystallinity, crystallographic orientation, nanoparticle size and distribution, and polycrystalline or single crystal configurations may be obtained.

3.2 Sample preparation

Although there are a multitude of molecules which exhibit spin crossover behavior, only a few are known to maintain stoichiometric and crystalline integrity when sublimated. $[Fe\{H_2B\,(pz)_2\}_2\,(bipy)]$ is one such molecule. Samples used in this study consist of multilayered thin film structures in a variety of different configurations. Substrates are either glass, as in the case of the sensors used for conductance testing, or silicon, as used for spectroscopy. Methods of depositing the thin films include thermal evaporation, magnetron sputtering, and Langmuir-Blodgette layer by layer deposition. Specifics will be outlined in the sections that follow.

3.2.1 Thin films of $[\mathbf{Fe\{H_2B\,(pz)_2\}_2\,(bipy)}]$

Unlike many spin crossover compounds, $[Fe\{H_2B\,(pz)_2\}_2\,(bipy)]$ maintains its crystal structure after sublimation. The first two studies to show successful sublimation [15], [16] used different techniques. Quandt et al. used a higher pressure environment of 10^{-2} mbar (0.075 Torr) to thermally deposit $[Fe\{H_2B\,(pz)_2\}_2\,(bipy)]$ at a temperature of 160°C onto a cooled glass substrate, while Palamarciuc used thermal deposition at a crucible temperature of 130°C with an ultra high vacuum 10^{-10} mbar (7.5x10^{-11} Torr) environment onto a room temperature substrate. These studies were followed by Dowben's group at the University of Nebraska [70] who used an ultra high vacuum enivronment similar to Palamarcuic and also confirmed that the molecule retains its spin crossover properties after sublimation into thin films.

The first logical step in this study was to develop a successful deposition process which would produce high quality, crystalline thin films of $[Fe\{H_2B\,(pz)_2\}_2\,(bipy)]$, in a repeatable manner, using the equipment available in our lab. After some testing in our high vacuum chamber, which also houses our magnetron sputtering system, we settled on using the high vacuum load-lock chamber which is part of our surface science characterization center. This

would allow for a high (10^{-8} Torr), or if needed ultra-high (10^{-10} Torr) vacuum environment, in situ characterization by scanning tunneling microscopy, e-beam substrate ablation, and a host of other capabilities.

A thermal evaporation crucible was installed on a high current feedthrough and was the temperature to voltage parameter was calibrated using a Hewlett Packard 6552A power supply and a Voltcraft thermometer with a K-type thermocouple. Once the temperature as a function of current (and time) was thoroughly characterized, 2342.2mg of $[Fe\{H_2B(pz)_2\}_2(bipy)]$ was placed in the crucible. A clean silicon substrate (University Wafer, <110> P-doped single crystal silicon) was placed 7cm above the crucible using a magnetically controlled manipulator arm. The crucible was heated to 120°C for 18min 24secs in order to produce a thin film of 150nm. X-ray diffraction on the resultant thin film

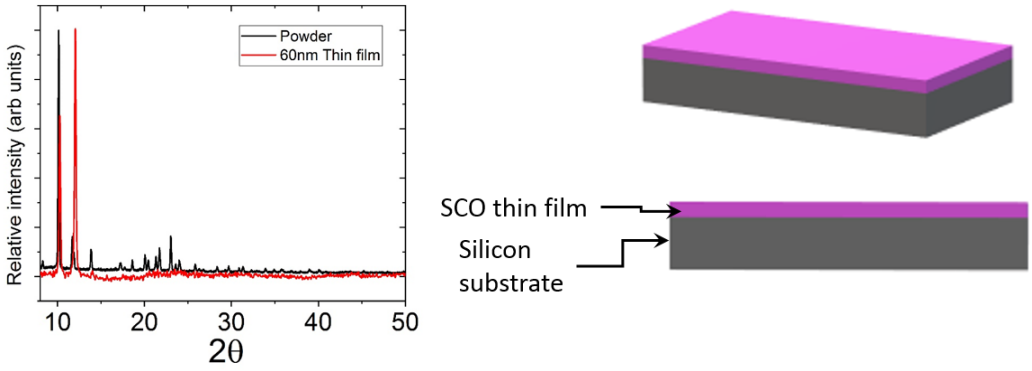

Figure 3.3. The first step in our study was to confirm the ability to create repeatable crystalline thin films of $[Fe\{H_2B(pz)_2\}_2(bipy)]$. In the x-Ray diffractogram shown above, a diffraction pattern for a 60nm thin film of $[Fe\{H_2B(pz)_2\}_2(bipy)]$ (shown in red) is superimposed upon the diffraction pattern of a powder sample (black), indicating better crystalline ordering in the thermally evaporated thin film than in the powder sample. Schematic representations of the sample are shown to the right.

showed more preferential crystalline ordering in the as-deposited thin film when compared to a diffraction pattern of the powder sample. Data was taken at the Integrated Nanosystems Development Institute (INDI) using a Bruker D8 Discover XRD machine.

3.2.2 Langmuir-Blodgett deposition of PVDF-HFP thin films

Following a method known from previous work in our lab [29] which is based on well known methods developed by Ducharme [71], PVDF-HFP in solution was suspended in a water subphase for layer by layer Langmuir-Blodgett (LB) deposition.

A solution of 0.05% by weight of PVDF-HFP in acetone was made by mixing PVDF-HFP powder with acetone and then heating to 80°C for 20 minutes to ensure complete solvation. This solution was then added to de-ionized milli-Q (18MΩ) water at 1.5μL per square centimeter of surface area for monolayer coverage of the water's surface. The substrate was then dipped by hand perpendicular to the surface of the water and allowed to dry in a commercial food dehydrator at 32°C. It has been shown and repeatedly confirmed that the best way to achieve β-phase crystalline ordering in PVDF and PVDF-TrFE thin films is by a thermal post annealing at around 130°C [20], [29], [55], [71], [72]. Slightly lower temperatures of around 120°C are shown to have optimal results for the copolymer PVDF-HFP [36], [37], although this is reported for μm scale films.

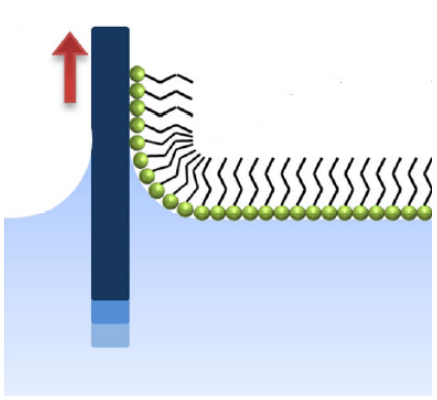

Figure 3.4. Monolayer control of thin film deposition can be achieved using the Langmuir-Blodgett layer-by-layer technique. Here the substrate passes through a monolayer of polymer which is suspended on the water. As the substrate is drawn through the polymer film, molecules from the film adsorb to the surface of the substrate. Illustration courtesy of Celestin[73].

This study utilizes both post annealed films and non annealed films, depending upon the configuration of the sample. For multilayered samples in which the PVDF-HFP is deposited before the $[Fe\{H_2B\,(pz)_2\}_2\,(bipy)]$, it is permissible to anneal the samples. For configurations

in which the PVDF-HFP must be deposited on top of the $[Fe\{H_2B(pz)_2\}_2(bipy)]$ thin film, the annealing temperature would damage the $[Fe\{H_2B(pz)_2\}_2(bipy)]$ films. This engineering issue has motivated another avenue of research in our lab, namely the optimization of the β-phase crystalline structure (ferroelectric properties) of PVDF without thermal treatments. Crystalline ordering for Langmuir-Blodgett vertically dipped substrates was confirmed with X-ray diffraction.

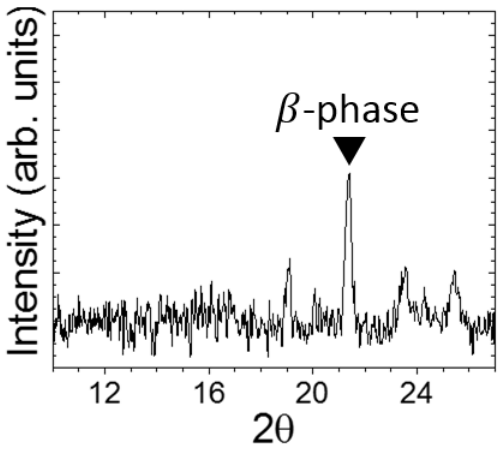

Figure 3.5. X-Ray diffractogram of a 60nm Langmuir-Blodgett PVDF-HFP thin film which has not received a thermal annealing treatment, shows a prominent peak at 21.2° 2θ , an indication β-phase crystalline ordering. Of the three crystalline phases for PVDF-HFP, the β-phase exhibits the most profound ferroelectric properties. Image courtesy of Ashley Dale.

In order to ensure that the PVDF-HFP films possess a switchable polarization, they were characterized using a Radiant Technologies Precision RT66B ferroelectric characterization system. For the data shown in Figure 3.4, a multilayered device consisting of a glass substrate with a bottom Ti electrode, the 60nm PVDF-HFP thin film, and a top Au electrode was constructed. The 80nm thick Ti electrode was deposited using magnetron sputtering and the top 80nm Au electrode was thermally deposited in high (10^{-7}Torr) vacuum. Thin gold wire leads connected the thin film electrodes to a sample stage circuit with conductive silver paint. The circuit has pins which are then connected to the Radiant Tech. RT66B via alligator clamps.

Another method which was used to pole the samples involved a removable adjustable top electrode. This device contains a copper plate attached to a micrometer stage which can be

precisely lowered to the top of a sample, taking the place of the top thermally deposited Au electrode.

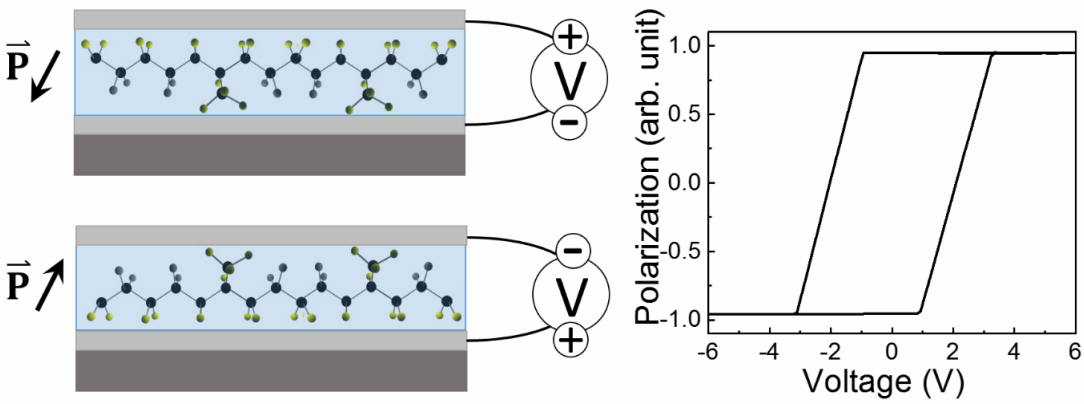

Figure 3.6. The normalized polarization measurements for voltage swept from -6V to 6V shows a clear hysteretic response indicating switchable ferroelectric ordering in a 60nm Langmuir-Blodgett PVDF-HFP thin film, as made in our lab, which has not received a thermal annealing treatment.

3.3 X-ray absorption spectroscopy

The fundamental process at work in X-ray Absorption Spectroscopy (XAS) is the promotion of a deep core level electron in a specific atom to an unoccupied state above the Fermi level by photoexcitation. The excited electron can then relax by decaying to a lower energy level, emitting photoelectrons, ejecting Auger and secondary electrons, or by the emission of a photon. This provides a direct measure of unoccupied density of states [74]. When using synchrotron radiation [75], XAS is a highly tunable, powerful method for determining specific electronic configuration, magnetic and geometric properties, and gathering information about the coordination environment of the selected atom.

3.3.1 X-ray electron interaction

The Hamiltonian describing the interaction of light with an electron is

$$\hat{\mathcal{H}}_{int} = -\mathrm{i}\hbar\frac{\mathrm{e}}{mc}\nabla\cdot\vec{A} + \frac{\mathrm{e}^2}{2m}\vec{A}^2 \tag{3.5}$$

in the weak field case the $\vec{A}^2$ term may be neglected giving a perturbing Hamilitonian of

$$\hat{\mathcal{H}}_1 = \frac{\mathrm{e}}{mc} p \cdot \vec{A} \tag{3.6}$$

$$\vec{A} = \hat{\mathrm{e}}_q A_\circ \cos\left(kx - \omega t\right) = \frac{1}{2}\hat{\mathrm{e}}_q A_\circ \mathrm{e}^{\mathrm{i}(kx-\omega t)} \tag{3.7}$$

where $\vec{A}$ is the vector field.

Fermi's Golden Rule describes the probability for transition by

$$W_{f\mathrm{i}} = \frac{2\pi}{\hbar} |\langle \Phi_f | \hat{T} | \Phi_\mathrm{i} \rangle|^2 \delta_{E_f - E_\mathrm{i} - \hbar\omega}, \tag{3.8}$$

$$\text{with the transition operator } \hat{T} = \hat{T}_1 + \hat{T}_2 + \hat{T}_3 + ... \tag{3.9}$$

representing all possible transitions. The first term of the expansion, T_1,is representative of a one-photon process and so describes x-ray absorption [74], and is equal to the interaction Hamiltonian allowing

$$\hat{\mathcal{H}}_1 = \hat{T}_1. \tag{3.10}$$

Taking the dipole approximation and considering the commutator

$$\left[\hat{\mathcal{H}}, \vec{r}\right] = \mathrm{i}\hbar \frac{p}{m} \implies \hat{T}_1 = \sum_q \left(\hat{\mathrm{e}}_q \cdot \vec{r}\right), \tag{3.11}$$

$$W_{f\mathrm{i}} \propto \sum_q \frac{2\pi}{\hbar} |\langle \Phi_f | \hat{\mathrm{e}}_q \cdot \vec{r} | \Phi_\mathrm{i} \rangle|^2 \delta_{E_f - E_\mathrm{i} - \hbar\omega}. \tag{3.12}$$

The dipole selection rule $\Delta l = \pm 1$ [76], for promotions of electrons from a core level with initial angular momentum l_i selects final states of $l = l_\mathrm{i} \pm 1$, allowing for transitions of the type $s \to p$, $p \to s$, $p \to d$, etc. Δl is given theoretically by both the matrix element between l_i and l_f, as well as by the final density of states [74]. Experimental observations have shown that it is more probable for $\Delta l = 1$, therefore making the transitions of the type $p \to d$ favored over $p \to s$.

3.3.2 X-ray absorption Spectroscopy of $[Fe\{H_2B(pz)_2\}_2(bipy)]$ on the Fe L_3 edge

The typical energy corresponding to the Fe L_3 edge is 708.11 eV, equal to the binding energy of a core $2p_{3/2}$ electron. Due to the splitting of the Fe frontier orbital, we instead see two distinct absorption peaks, one at 708.9 eV corresponding to the t_{2g} suborbital, and another at 710.7 eV for the e_g orbital as shown by the energy diagram in Figure 3.1. These energies have been confirmed for $[Fe\{H_2B(pz)_2\}_2(bipy)]$ by several previous studies [17], [57], [77].

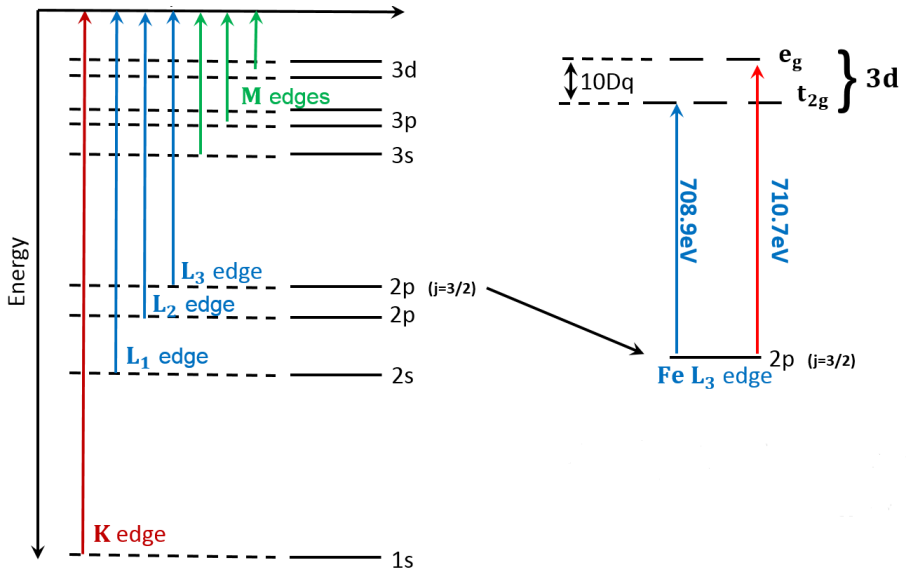

Figure 3.7. Energy diagram showing the origin of the K, L, and M edges which constitute signature energies for an electron transition in X-Ray absorption spectroscopy. In the case of an octahedral transition metal coordination compound such as $[Fe\{H_2B(pz)_2\}_2(bipy)]$, the $3d$ orbital is split into two suborbitals, the t_{2g} and the e_g, which have transition energies (708.9eV and 710.7eV respectively) slightly different than the typical FE L_3 edge.

3.4 XAS at Beamline 6.3.1 Advanced Light Source, Lawrence Berkeley Laboratory

X-ray absorption was done at the Advanced Light Source (ALS) at Laurence Berkeley National Lab, Berkeley California, on the bend magnet magnetic spectroscopy beamline 6.3.1. The ALS is a synchrotron light source capable of 1.9GeV beam energy. Thermionically emitted electrons are accelerated in a linear accelerator and then injected into a booster ring

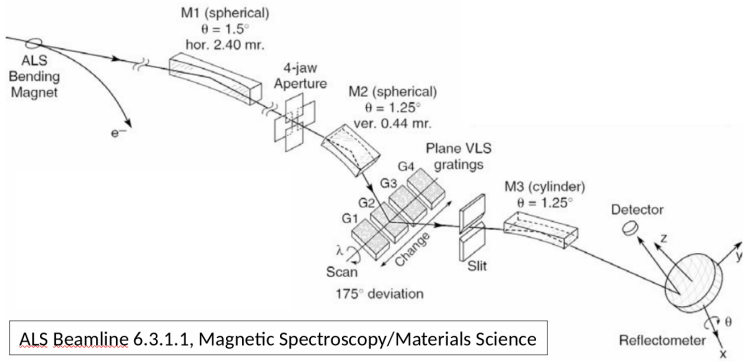

Figure 3.8. A basic schematic of the ALS beamline 6.3.1 showing the path of photons tangentially harvested off of accelerated electrons in the storage ring to the detector. The photons will pass through a series of mirrors and gratings which will focus the beam and select the desired energies [78].

where they undergo acceleration to relativistic speeds. Finally they are moved to a 200m diameter storage ring where x-rays are harvested at points tangential to the ring making up the 40 beamlines at which various experiments are conducted.

X-ray absorption spectroscopy, in total electron yield (TEY) mode at the Fe L_3 edge, was used to probe the unoccupied Fe weighted e_g and t_{2g} molecular orbitals of $[Fe\{H_2B\,(pz)_2\}_2\,(bipy)]$, as a function of the ferroelectric polarization of the adjacent PVDF-HFP thin film. This provided a clear picture that the spin state of the $[Fe\{H_2B\,(pz)_2\}_2\,(bipy)]$ thin film depends upon the polarization direction of the PVDF-HFP layer. Measurements were done at the Advanced Light Source at Lawrence Berkeley National Laboratory on bending magnet beamline 6.3.1, with TEY mode configured using circularly polarized, positive helicity photons with a photon flux of 10^{11} photons/sec/0.1 %BW (BW = Beam Width). These parameters are the same as used in prior studies [57], [58], [79], [80]. The intensity of the X-ray beam was tuned in order to limit photoactivation of the molecule yet maintain an acceptable TEY signal [63].

3.4.1 Total electron yield mode: Basic working principles

Rather than recording x-ray absorption and transmission via direct measurement such as measuring transmitted and incident x-rays, which require specific sample thickness, indirect

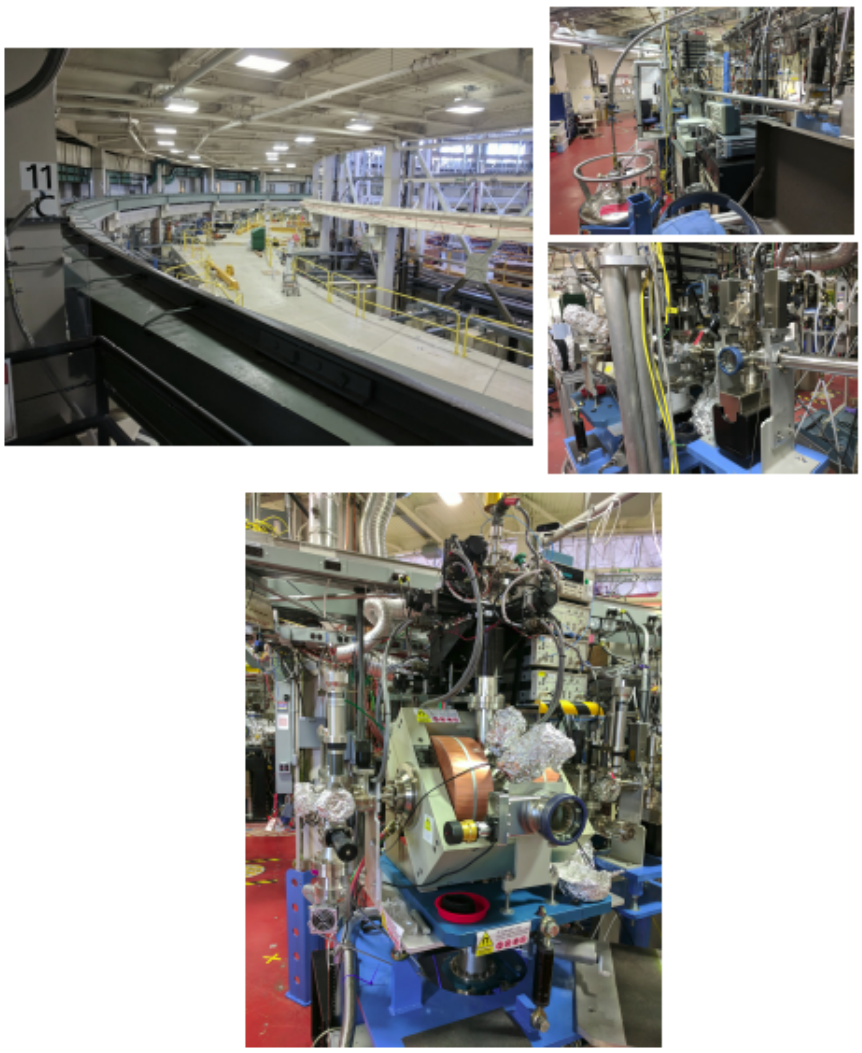

Figure 3.9. Top left: The electron storage ring at the ALS. After the electrons leave the booster ring they are kept in the storage ring and accelerated to near-relativistic speeds. Tangent to this ring are multiple stations which utilize x-rays harvested from the accelerating electrons. The two images on the right show par of beamline 6.3.1.1, which houses soft x-ray experiments such as XAS. In the bottom center photo the main experiment chamber which houses the XAS sample holder, detection, temperature control, and magnetic equipment.

methods are used. These include x-ray fluorescence yield, which looks at radiative decay of excited electrons, and two complimentary surface drain current techniques, Auger and total electron yield (TEY). The Auger process, illustrated in Figure 3.11, causes the ejection of an outer shell electron, via electron decay into a vacant inner shell, to restore energetic

equilibrium in a photoexcited atom. This process is species specific, and highly dependant on the energy level configuration of the atomic orbitals.

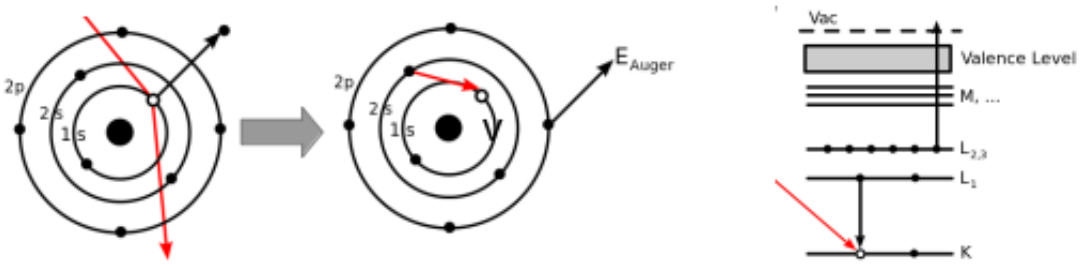

Figure 3.10. The Auger process. From left to right: A photoexcited electron is ejected from the core level of an atom. This results in relaxation by an electron from a higher energy level causes a subesquent ejection from an outer shell electron. The energy involved in this process is highly species-dependant, therefore giving a unique spectroscopitc signature. Image credit: By A. Carlson - Own work, Public Domain, https://commons.wikimedia.org/w/index.php?curid=3195660

In TEY, excited photoelectrons from core orbitals transition above the vacuum Fermi level to higher energy states. The resultant decay produces an Auger cascade which in turn excites other electrons to the surface of the material. The combination of excited Auger electrons and so-called secondary excited electrons on the surface are measured as a drain current with a picoammeter. The current intensity changes as resonant energy levels are excited in the material with the sweeping action of the incident photon energy by the synchrotron source. TEY is a surface sensitive technique, and provides good local information by directly probing the electron population of a given orbital [75], [81]–[83].

3.5 Charge transport measurements of molecular $[Fe\{H_2B(pz)_2\}_2(bipy)]$ thin films: Experimental setup

The main focus of this study centers around the ability to use external voltage to control the spin state, and thus the conductivity of the spin crossover layer in a multilayered system, in effect creating a multiferroic gated electronic device. First observed in 2009 [84], a handful of studies have characterized electron transport changes with spin state change of SCO materials in single crystals [85], powder [86], thick films [87], thin films[88], [89], nanoparticles

[90], and even single molecules [43], typically using temperature or light to induce the phase transition. While temperature and light have a global effect on the overall environment of the sample, the advantage of developing a method to change the spin state of the SCO material with a ferroelectric is the possibility of local control of the polarized environment of the molecule, leading to the ability to address very small, local regions on a sample. Most data shows that there is an increase in conductivity in the HS state, likely due to the absence of the pairing energy for the 2 unpaired electrons in the t_{2g} suborbital, allowing for an easier migration of unpaired electrons into the conduction band [91].

The most direct approach to inducing a spin crossover transition in $[Fe\{H_2B\,(pz)_2\}_2\,(bipy)]$ is to lower the temperature of a thin film sample below the transition temperature of 160K. Conductivity measurements as a function of the thermal SCO can then be characterized.

To do this, a device needed to be developed that can be connected to the proper testing apparatus. Several device configurations were tried using multiple approaches. As shown in Figure 3.11, photolithography was used to mask off two distinct electrodes with a gap of 35μm and a 125nm thin film of $[Fe\{H_2B\,(pz)_2\}_2\,(bipy)]$ was then deposited in the interstitial region. The method proved to be inferior, and produced either current levels which indicated an open circuit, or on some samples a short circuit. The 35μm gap is most likely to wide to detect any appreciable current, let alone a current change.

Current is measured with a Keithley 6487 picoammeter/source meter interfaced to a PC for control and data collection with Lab View software. The devices are connected to the picoammeter using high purity gold wire fastened with conductive silver paste. Shown in Figure 3.12, the sample rests on a copper plate fixed to a stage made of Delrin, an acetal (polyoxymethylene) material which is highly machinable, and known to dissipate static charge. Care was taken to shield all leads to reduce noise from ambient electromagnetic interference.

The Delrin block was milled to accept the copper plate flush with it's surface, and a pocket was milled underneath the copper plate as a reservoir for cryogenic liquid, in this case liquid nitrogen. Two holes were then drilled and tapped for 3/8-16 NPT pipe fittings to serve as the inlet for the cryogenic fluid on one side of the pocket, and an exhaust on

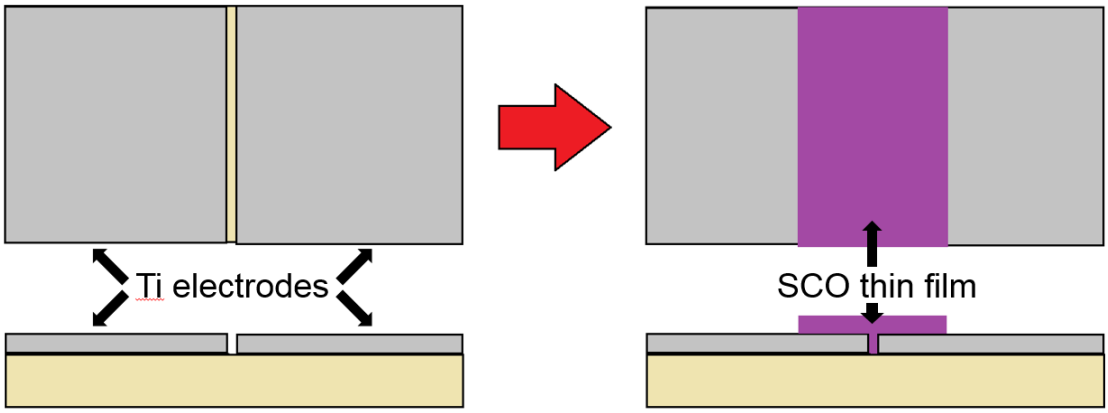

Figure 3.11. A diagram of the first device made to make conductivity measurements of a $[Fe\{H_2B\,(pz)_2\}_2\,(bipy)]$ thin film as a function of temperature, in an attempt to show an abrupt change in conductivity with spin state change. Two Ti electrodes were separated by a 35μm gap created by photolithographic masking.

the other. A K-type thermocouple was secured to the copper plate to monitor temperature. Holes were also drilled and tapped in the top surface of the Delrin block to secure a circuit board which serves as a junction between the gold wires from the sample and the leads to the Keithley 6487 picoammeter. Small grooves were milled to accept wires and a cover was fitted to protect the wires.

The first conductivity tests using the titanium electrodes separated by a 35 μm gap made it immediately apparent that these tests need to be carried out in a controlled atmosphere, as frost quickly grew on the face of the sample as the temperature dropped below the freezing point of water. The Delrin test block was then put inside a nitrogen atmosphere, which eliminated any frozen water upon cooling or condensation upon warming, well below the transition temperature of the SCO material.

To deal with the issue of a weak signal from the sample, it was decided to increase the surface area of the electrodes by incorporating an interdigitated electrode design into the sensor. The first attempts at this method consisted of designing a pattern for a photolithographic mask in Auto-CAD and using the photolithography lab at INDI (Integrated Nanosystems Development Institute) to make a pattern onto which we could deposit a conductive thin film, and then wash away the mask to leave the desired electrode configuration. Even though

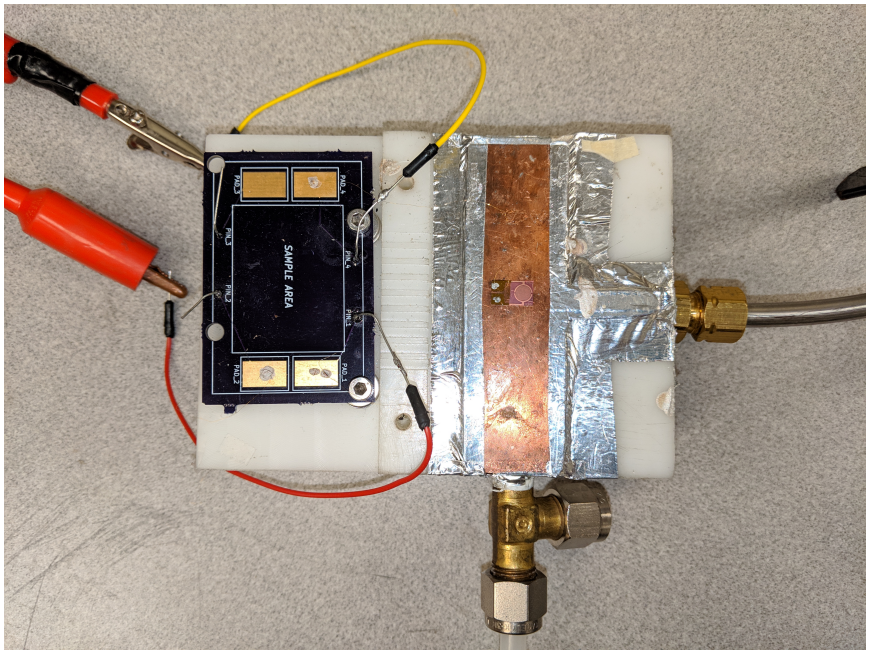

Figure 3.12. The lab built sample stage used in conductivity measurements. It is capable of taking variable temperature measurements from ambient temperature down to about 193K. During measurements which fall below 273K, it is placed inside a chamber in order to control the atmosphere.

interdigit spacing of 20 μ m were achieved, washing away all of the mask proved difficult, and it was not possible to consistently make sensors that exhibited a similar background current measurement. This was due to residual metallic material left in between the electrodes.

Proprietary sensors were ordered from NanoSPR sensor company. These are interdigitated sensors with gold electrodes spaced at 20 μm. It was possible to deposit SCO material on them and take measurements, but again weak signal and in some cases inconsistent background reading were encountered.

Finally, sensors were ordered from MicruX, Inc.. These sensors have one pad consisting of 90 pairs of gold interdigitated electrodes which were 250nm thick, 10 μ wide, and spaced at 5 μm. These dimensions were measured, checked and confirmed in our lab using optical microscopy. They are of high quality and yielded very consistent background readings, and negligible leaking current. The sensors proved to be reliable and able to sense sub-nanoampere currents with much higher signal to noise ratio than the previous configurations.

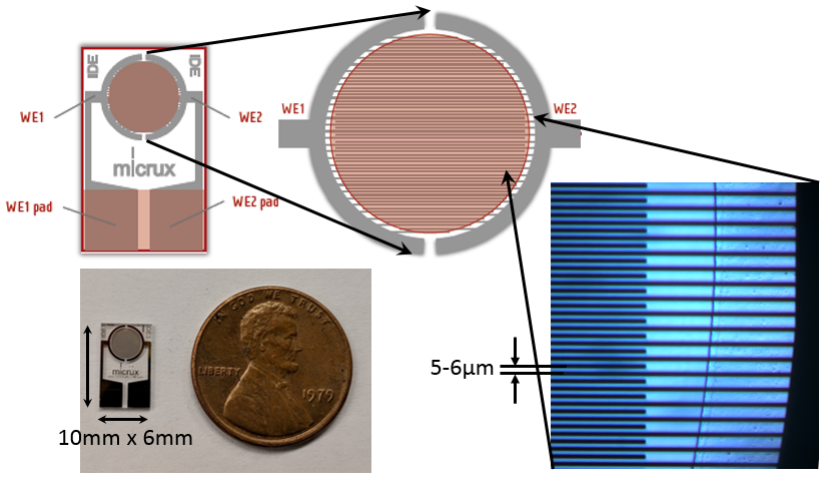

Figure 3.13. Interdigitated sensor manufactured by MicruX, Inc. This high quality sensor consists of a circular pad with an array of interdigtated Au sensors 150nm high with a spacing of 5μm on a glass substrate. The MicruX sensor proved to be very reliable and was capable of measuring very low, sub-nanoampere currents with very little current leaking.

For a typical measurement to characterize conductivity as a function of spin state, the SCO thin film is deposited directly on top of the MicruX interdigitated sensor. The thin films are grown in a high vacuum of 3.4 x 10^{-8} Torr at a rate of 0.15 $^{nm}/_{s}$, as outlined in Section 3.1.1.

The samples are electrically connected to the picoammeter as shown in Figure 3.13. Care is taken to shield all wires as well as possible, and the setup is isolated from disturbances such as people walking by or stray magnetic fields from other lab equipment during measurements [92]. For temperature dependent tests, the voltage is typically swept from between -10V to 10V in steps of 0.5 V for a given temperature. This takes about 2 minutes to complete. The temperature is then lowered and allowed to stabilize before the next voltage sweep.

The next tests that were performed consisted of measuring conductivity change as a function of ferroelectric polarization induced spin state change. To do this, a multilayered structure was created on the MicruX sensors as shown in Figure 3.12. First, the SCO material was thermally deposited as before, using the known parameters for vacuum and deposition rate. A ferroelectric PVDF-HFP thin film was then deposited using the Langmuir-Blodgett technique as described above. It is important to note that the PVDF-HFP thin films are

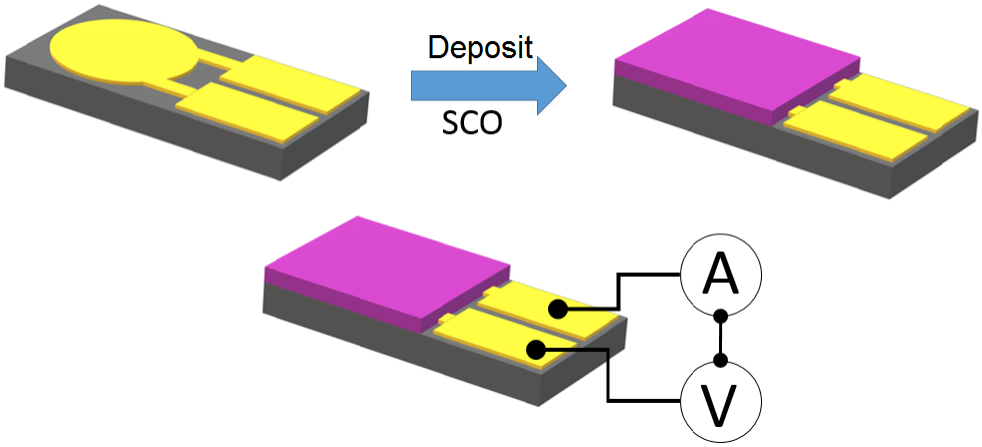

Figure 3.14. Flow diagram for the production of a sample for simple conductivity testing. The SCO thin film is thermally deposited directly onto the MicruX interdigitated sensor. The desired voltage is then swept across the electrodes while the current response is measured by the Keithley 6487 picoammeter.

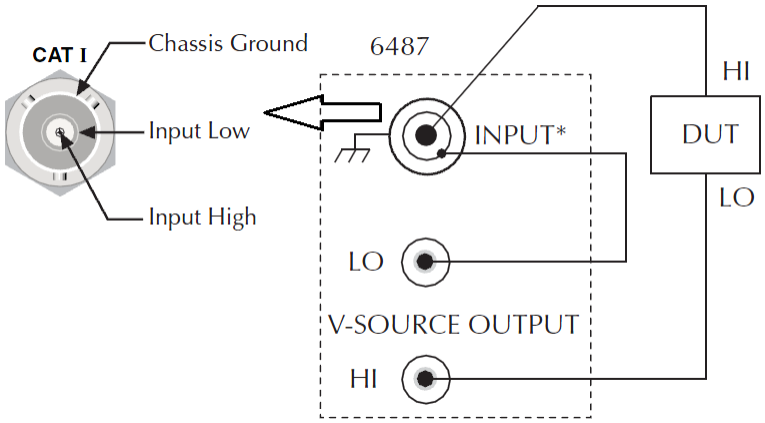

Figure 3.15. The electrical schematic for conductivity testing using the Keithley 6487, as re-printed from the Keithley 6487 Reference Manual. The Device Under Test (DUT), in our case the MicruX sample, is wired in series with the source and picoammeter [93].

not post annealed, as annealing was seen to damage the underlying SCO thin film. The ferroelectric was then poled using two different methods. In method one, the ferroelectric was poled by using the poling device with a removable top electrode as described above. The top electrode was lowered on top of the sample until it was just in contact with the PVDF-HFP thin film. A poling voltage (depending upon the desired polarity of the sample)

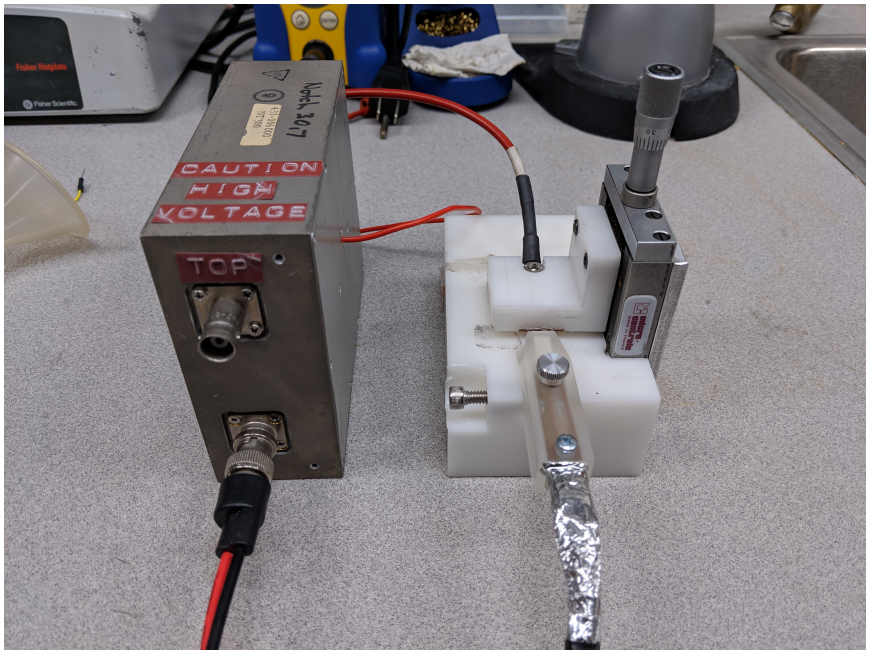

Figure 3.16. The lab-built poling station used to switch the polarization of the ferroelectric PVDF-HFP thin film by using a removable top electrode. The electrode is mounted to a slide which can be adjusted by a micrometer, allowing for precision positioning of the top electrode.

of ±30V was then applied. In order to minimize back-switching in the ferroelectric, the voltage was ramped up over a reasonable time scale of about 1 $^{V}/_{s}$, allowed to saturate for 2 minutes, and then ramped back down at the same rate to prevent back-switching of the ferroelectric domains. Note that a poling voltage of 30V, in this geometery, is equivalent to an electric field of roughly 360 $^{MV}/_{m}$ parallel to the plane of the sample. This is well above the coercive voltage required for creating a single poled ferroelectric domain in PVDF-HFP, which is 100 $^{Mv}/_{m}$.

In method number 2, a conductive Au pad was thermally evaporated on top of the PVDF-HFP thin film. The deposition took place under high vacuum with a base pressure of 2.8 x 10^{-8} Torr with a deposition rate of 0.05 $^{nm}/_{s}$ on an area directly above the interdigitated electrodes which was masked by aluminum foil to yield a conductive pad of 80nm thick. The poling pad was then connected to a voltage source via high purity Au wire attached with silver conductive paint. The interdigitated electrodes were used as the bottom poling

electrode. A poling voltage of ±30V was then applied in the same manner as outlined above to avoid backswitching of the ferroelectric.

4. DATA AND DISCUSSION

4.1 The thermal transition, x-ray absorption spectroscopy data and discussion

In order to check if the spin crossover behavior was retained in the thermally deposited thin films, XAS was employed. Samples (see figure 4.1) were made consisting of a 60nm thin film of $[Fe\{H_2B\,(pz)_2\}_2\,(bipy)]$ deposited on a silicon substrate ($<110>$, p-doped single crystal, University Wafers). The Si substrate was cleaned by using the standard procedure as outlined above, and was untreated and so retained it's native oxide layer.

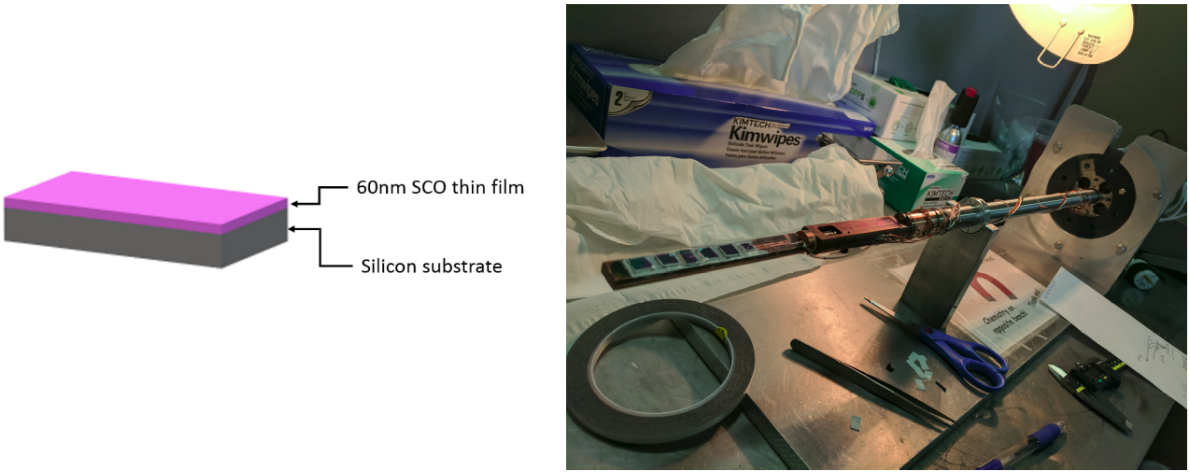

Figure 4.1. The diagram on the left shows the configuration of samples used to check for thermally induced spin crossover by characterization with XAS. 60nm thin films of $[Fe\{H_2B\,(pz)_2\}_2\,(bipy)]$ were deposited on Si substrates. On the right is a photograph of the variable temperature sample holder for XAS TeY mode. There are two thermocouples present on the sample holder a known distance apart, allowing for accurate calculation of the sample temperature.

After mounting to the XAS TeY holder with conductive silver paste, the holder was placed into a degassing chamber for 24hrs. The sample holder was then placed into the experiment chamber on beamline 6.3.1.1 and allowed to pump down to a terminal pressure on the order of low 10^{-8} Torr. Proper calibration was performed to align the instrument for XAS, the 1200 line grating was chosen, a photon exit slit of 20 μm, negative circularly polarized light with an aperture of 0.500 mm. The energy was swept from 680 eV to 715 eV. A single scan took approximately 15 seconds.

The first scans, at room temperature (297K) showed the molecule to be in a mostly HS state. Liquid nitrogen was introduced in order to lower the temperature while a heater system controlled by a proportional integral derivative (PID) device. When changing the temperature, it was necessary to wait about 15 minutes for the system to stabilize. The system was surprisingly stable, exhibiting minor fluctuations of few tenths of a Kelvin during measurements.

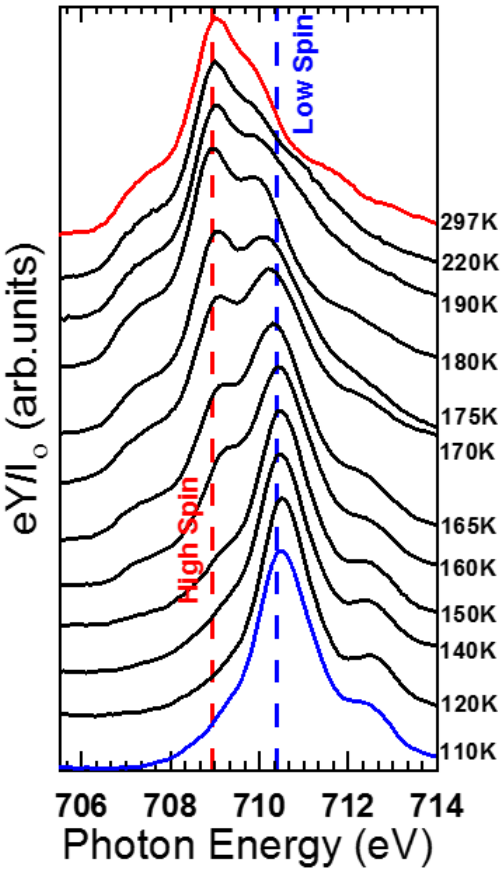

Figure 4.2. The shift in excitation energy peaks in this XAS data shows a clear thermally induced transition in the 60nm $[Fe\{H_2B\,(pz)_2\}_2\,(bipy)]$ thin film deposited on a silicon substrate. The peak shifts from 711 eV at low temperature, signifying a population of the t_{2g} to a mixed state and then to mostly populated high spin e_g and t_{2g} at room temperature.

At 297K, a single, distinct peak is noted at 708.9eV showing the partial population of the t_{2g} suborbitals with unpaired electrons indicating the S=2 High Spin (HS) state. The peak has a sharp rise from 708eV to the point at 708.9, and then a more gradual decent down past

711eV, with a slight hump at 710.7eV. This points to a percentage of the molecules being in the S=0 Low Spin (LS) state as now the e_g suborbital is completely populated. The LS state peak begins to become well defined at 190K and is seen as a separate peak with equal intensity at around 175K. This indicates equal populations of LS and HS states and signifies T_{12}.

Below T_{12} the t_{2g} suborbital quickly depopulates and the e_g suborbital populates, yielding a mostly LS state system as the temperature dips below 140K. Since the energy of the system is proportional to temperature

$$E \propto k_b T. \tag{4.1}$$

By considering the density of states as a function of temperature, it is possible to gain an understanding of the energetics involved in switching from the HS state to the LS state by different mechanisms, *eg.* light, temperature, or electric field. This could give insight into the nature of the transition and its connection to the molecules local environment.

4.1.1 Ferroelectric polarization dependent switching of the spin state

Samples in the schematic configuration shown in figure 4.3 were analyzed with XAS in order to characterize the influence of an adjacent polarized ferroelectric substrate on the spin state of the SCO material. These samples consisted of a silicon substrate, 80nm titanium bottom electrode, a 20nm Langmuir-Blodgette thin film of PVDF-HFP, and a 60nm $[Fe\{H_2B(pz)_2\}_2(bipy)]$ thin film. A removable top electrode, as described in experimental methods was used to pole the samples. The poling took place approximately 24 hours before these measurements were taken. Poling of the ferroelectric layer was accomplished by applying 10V, which created an electric field of approximately 120 MV/m perpindicular to the plane of the sample. It should be noted that this is well above the coercive field (100 MV/m) required to created a single polarized domain in PVDF-HFP [37].

Figure 4.4 shows definitively that when the molecular thin film $[Fe\{H_2B(pz)_2\}_2(bipy)]$ is adjacent to the molecular ferroelectric PVDF-HFP, non-volatile locking of the spin state into the low spin state configuration may be achieved, well above the thermal transition

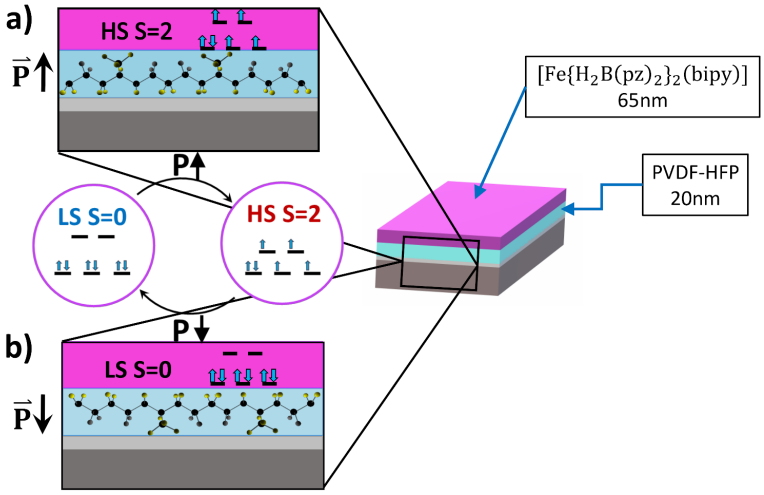

Figure 4.3. Schematic representation of samples used to characterize spin state coupled to a polarized ferroelectric substrate with XAS. The composition of the structure is as follows: Silicon substrate, bottom electrode of 80nm titanium, 20nm PVDF-HFP layer, 65nm of $[Fe\{H_2B\,(pz)_2\}_2\,(bipy)]$. The thickness of the PVDF-HFP layer in the diagram is exaggerated to show a clear picture of the conformation of the ferroelectric polymer chain in different polarization directions. Figure **a** shows the molecule in the HS S=2 state while the PVDF-HFP is poled up, while **b** shows the LS S=0 state as the PVDF-HFP is poled down [63].

temperature of 160K [79] . This serves as a write function, and therefore has many important implications for the use of organic, molecular thin films as components in next-generation memory devices [94]. In this example, the ferroelectric was poled more than 24 hours before the samples were characterized by XAS. There is reason to believe that the effect could be stable for much longer periods of time, as the polarization of PVDF based ferroelectric polymers is very stable.

This data points to an acute interaction between the SCO material and the ferroelectric at the interface. Previously, this interaction has been seen to be relevant for only a few molecular layers (less than 12nm) of the $[Fe\{H_2B\,(pz)_2\}_2\,(bipy)]$ [57], while the data in Figure 4.4 may hint at a somewhat longer interaction length [63], [79]. This could be due to a more ordered β-phase in the PVDF-HFP than in the PVDF-TrFE thin films used previously, or a higher local electric field due to better polarization of the PVDF-HFP sample. The PVDF-HFP

films could also posses less pinholes and better crystallization, which an active study in our lab will address.

In fact this is a question that deserves further attention, and a thorough study of side by side testing of samples made with the two co-polymers in the same lab may be called for, as improved crystallization is crucial for the observation of this polarization effect. Lack of crystallization diminishes the net dipole moment at the surface due to the random distribution of dipole moments and the absence of a single poled domain [63], [95], [96] The spin crossover phenomena is associated with changes in the electronic configuration of the molecule due to the energetic splitting of the molecular frontier orbitals into the e_g and t_{2g} suborbitals. The influence of the local electric field due to the polarization of the ferroelectric substrate must indeed be significant in order to push the molecule into the low spin state at above it's transition temperature.

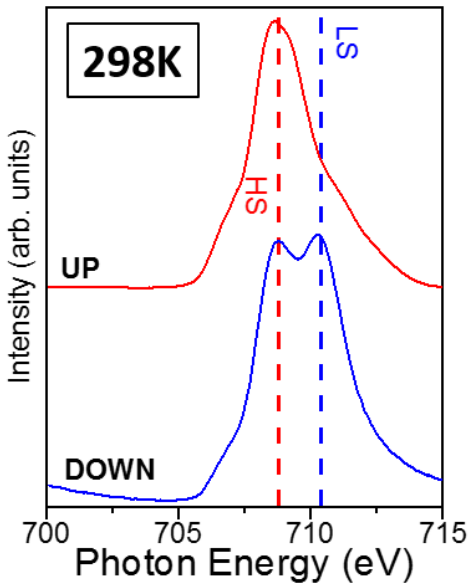

Figure 4.4. XAS data showing a room temperature contrast of the spin states for two separate polarization configurations. The SCO layer adjacent to the ferroelectric layer which is polarized up, or towards the SCO layer shows a majority HS state, while a mixed state with a significant portion of the material in the LS state is present in the sample with the ferroelectric poled down, or away from the SCO layer.

Looking at the XAS data of the polarized samples as a function of temperature gives a clear picture of the evolving density of states for the t_{2g} and e_g sub orbitals in the different

electric fields during temperature change. This allows for the energetics involved in the electric field induced spin state transition between HS and LS states to be measured. The inset between panels **a** and **b** in Figure 4.5 show deconvulted spectra for the up polarized sample at 200K and the down polarized sample at 298K. The deconvolution of the respective spectra for each substrate through the entire temperature range allows for comparable LS to HS ratios, or γ_{LS} to be chosen and analyzed.

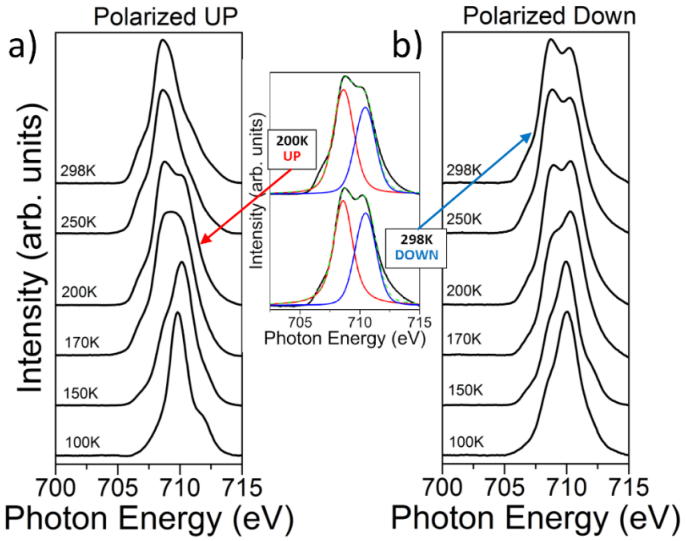

Figure 4.5. x-ray absorption spectra showing the changing intensities of the e_g and t_{2g} features for $[Fe\{H_2B(pz)_2\}_2(bipy)]$, as a function of temperature and substrate ferroelectric polarization. In **a**, the PVDF-HFP substrate is polarized up or toward the SCO layer. In **b**, the PVDF-HFP substrate is polarized down or away from the SCO film as unoccupied states of the e_g orbital above the transition temperature are observed, indicating that the sample can be locked into the low spin S=0 state past the transition temperature of 167 K. Each spectrum is deconvoluted into t_{2g} (red curve) and e_g (blue curve) peaks, shown in the inset between **a** and **b**.

The comparable temperature for a γ_{LS}=1 value is at 170 K for up polarization and 250 K for down, or a temperature difference of 80 K. A Complete graph of the data illustrating the relationship of γ_{LS} to temperature and polarization is shown in Figure 4.6 **a**, along with, in panel **b**, γ_{HS} vs temperature and simulation data from the Ising model described in Section 2.3, p.36 *Model to examine the energy difference of the spin state transition.*

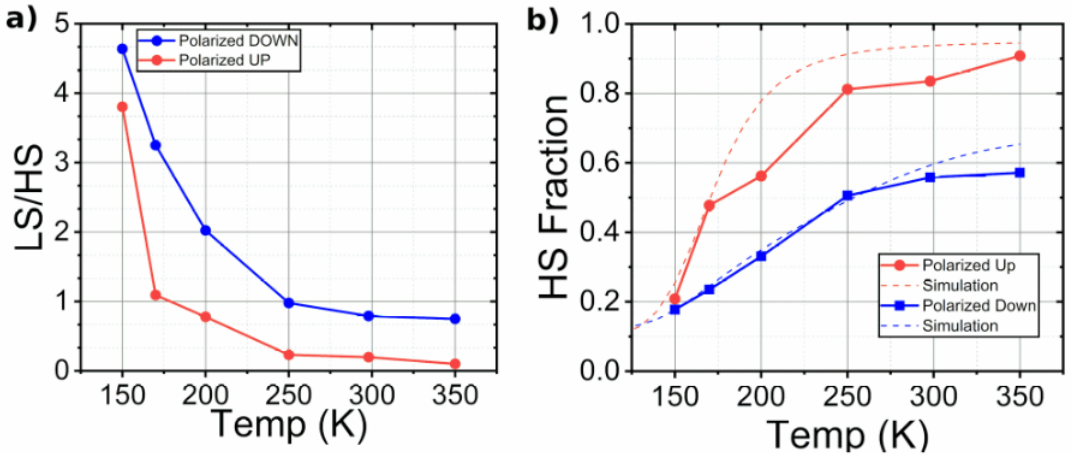

Figure 4.6. Comparable ratios of low spin (LS) state to high spin (HS) state for different temperatures and polarization, as measured by XAS on Device 1. Figure 3a is a plot of (LS/HS ratio) as a function of temperature for two different polarized directions, as derived from the XAS spectra; the red data curve is for the ferroelectric PVDF-HFP polarized up and the blue data curve is for PVDF-HFP polarized down. HS Fraction as a function of temperature is plotted in b, with the modified Monte Carlo Ising model simulation superimposed [63].

This Hamiltonian is used with Monte Carlo methods, developed and computed by Ashley Dale, to provide simulation data which is shown in Figure 2.4. Data indicates that the polarization of the ferroelectric substrate in the up configuration gives an activation energy difference $\Delta_\circ$ between the HS and LS states of 88 meV, while when the ferroelectric substrate is poled up, or towards the SCO layer. The energy difference parameter $\Delta_\circ = 198$ meV when the ferroelectric substrate is poled down, or away from the SCO layer. The energy difference parameter between the two polar conformations of the substrate, according to simulation, is seen to be 110 meV [63].

The polarization contingent energy difference seen in $\Delta_\circ$ points towards significant substrate-dependant changes within the $[Fe\{H_2B\,(pz)_2\}_2\,(bipy)]$ thin film. While the substrate has, in previous studies, shown to produce or affect spin state bistability, here it clearly shows a reliance on ferroelectric polarization direction [17], [18], [57], [63], [79], [80], [97].

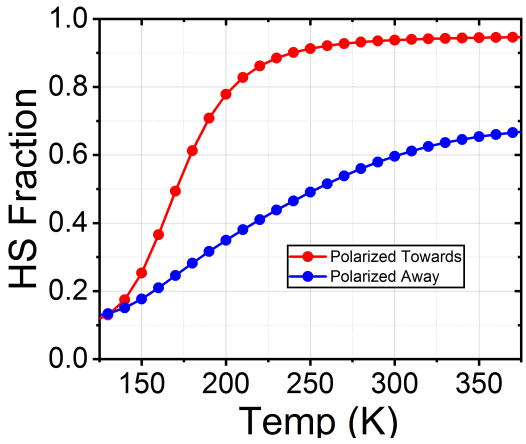

Figure 4.7. A Monte Carlo simulation using the Hamiltonian (2.60) shows HS fraction γ_{HS} as a function of temperature for a multi-particle spin crossover system in contact with a polarized (ferroelectric) substrate. Activation energy for the HS→LS transition may be deduced by considering similar HS fractions at different polarizations of the substrate. Here we see that for a substrate polarized up, $\Delta_\circ$=88 meV while for a substrate polarized down. $\Delta_\circ$=198 meV, indicating a difference of 110 meV between the two configurations. Data produced by Ashley Dale, as published in [63]

4.1.2 Conductivity change with spin state switching

Electrical transport change with spin state change is well documented in SCO materials, however, to date the non-volatile conductance switching of SCO molecules in the presence of a large electric field, or polarized environment has just recently been characterized by our group [63], [79], [94], [98]. The conventional route to characterizing conductance change in a spin crossover thin film is through temperature change, and here it is no different. After temperature dependant current data is shown, data for a non-volatile switching of the conductance will be presented.

4.1.3 Spin crossover and conductance change via the thermal transition

Once again, the most direct way to induce the SCO transition is through temperature change, so as a proof of concept temperature was varied from 298K to 140K while taking conductivity measurements as outlined in Section 3.5, p.50, using a MicruX 5 μm inter-

digitated sensor. Figure 4.7 shows the recorded data for temperature dependant current measurements as a function of voltage. The 298K data shows a clear non-ohmic response. Below the transition temperature $T_{1/2}$, at 150K, a change in conductivity of about 2 orders of magnitude is observed, indicating an absence of unpaired electrons in the e_g suborbital, consistent with larger highest occupied molecular orbital to lowest unoccupied molecular orbital gap of $[Fe\{H_2B\,(pz)_2\}_2\,(bipy)]$ and the resulting low conductance in LS states noted [52], [79].

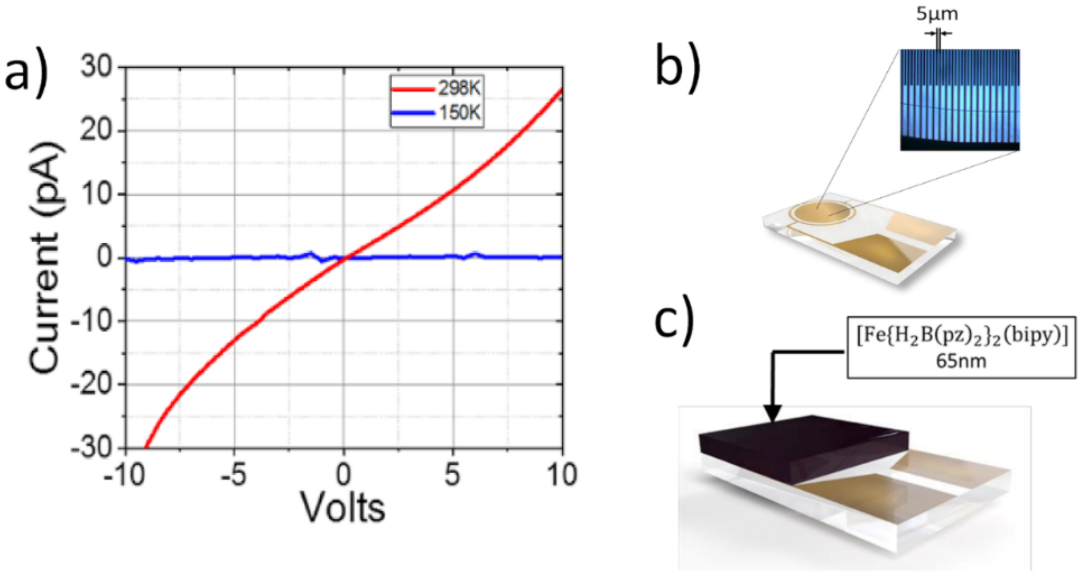

Figure 4.8. The differences in conductance for [FeH2B(pz)22(bipy)] thin films for the high spin (HS) dominated state verses the low spin (LS) dominated state. Figure a shows the conductance measured across Device 2 at room temperature (298 K) and below , the transition temperature (150 K). Interdigitated electrodes with a spacing of 5µm were used as the basis for all transport measurement, as shown in b. As shown in c, Device 2 consists of a [FeH2B(pz)22(bipy)] thin film deposited directly on interdigitated electrodes.

4.1.4 Polarization dependent conductivity change with spin state transition

Room temperature, non-volatile voltage controlled spin state switching, and subsequent change in conductivity, could be the missing piece to next generation electronic devices. In the case of a molecular thin film such as $[Fe\{H_2B\,(pz)_2\}_2\,(bipy)]$ this requires a read and a write function, which is the accompanied electrical conductivity change.

XAS data compellingly demonstrates the polarization dependent spin state change in $[Fe\{H_2B(pz)_2\}_2(bipy)]$, and now recently a demonstration of the accompanying conductivity change has been characterized.

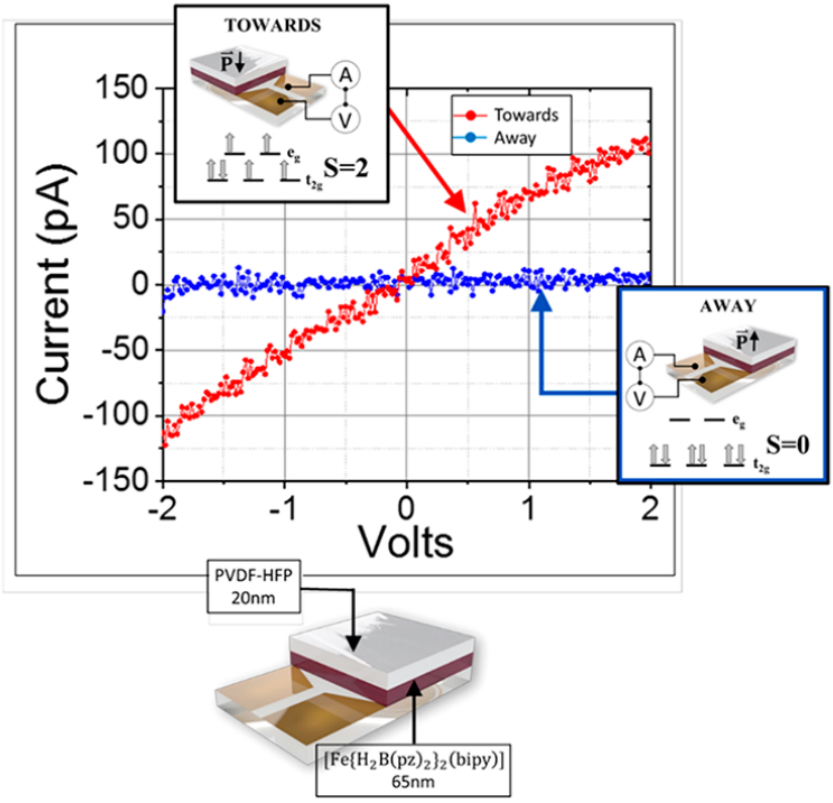

Figure 4.9. Spin dependent conductivity controlled by the polarized environment of the $[Fe\{H_2B(pz)_2\}_2(bipy)]$ SCO thin film. The corresponding XAS spectra at room temperature of representative samples with the ferroelectric poled "up" and "down" are included to illustrate electronic configuration in each situation [79].

Figure 4.8 shows polarization dependent conductivity data for the SCO material $[Fe\{H_2B(pz)_2\}_2(bipy)]$. Samples were prepared in the manner outlined in Section 3.1.2 p.40 and Section 3.5, p.50 and have the following parameters: a 65nm thin film of $[Fe\{H_2B(pz)_2\}_2(bipy)]$ is deposited directly on top of a $5\mu m$ MicruX interdigitated sensor, approximately 10nm of PVDF-HFP was then deposited, using the Langmuir-Blodgette technique, on the $[Fe\{H_2B(pz)_2\}_2(bipy)]$ thin film.

A removable electrode was placed in contact with the top of the PVDF-HFP thin film. While interdigitated gold electrodes were used as the bottom poling electrodes together with the top removable electrode, this created a coplanar poling environment for the ferroelectric. ±10VDC was applied to pole the ferroelectric either up or down. The voltage was carefully ramped up and down to prevent back-switching of the ferroelectric layer. The external coercive field was then removed before conductivity tests were taken. I-V curves were taken using the electrical testing setup described in Section 3.5, p.50.

A conductance change of two orders of magnitude is observed between the two different polarizations. As was mentioned previously, there is a difference in energy between the HOMO and LUMO bands of about 2eV in $[Fe\{H_2B(pz)_2\}_2(bipy)]$ for the LS state, which is consistent with the observation of a higher conductance for the HS state on the up polarized ferroelectric substrate.

The configuration of the sample in Figure 4.8 is essentially a top and bottom gated transistor-like structure, with a non-volatile state component. The write function is the non-volatile voltage control of the spin state. The read function is the current sensing of the spin state. This demonstrates the viability of spin crossover materials as molecular multiferroics with device capability.

This study has given a clear demonstration of the isothermal, bistable, non-volatile switching of both the spin state and conductance in a molecular thin film of $[Fe\{H_2B(pz)_2\}_2(bipy)]$ when deposited on a ferroelectric PVDF-HFP substrate. This switching occurs by the application of a voltage, and a sensing current, here on the order of picoamperes, reads off the spin state. XAS and theoretical modeling, in the form of a modified Ising model, have given insight into the switching mechanism and the energy involved. Separation of the energy gap between the HS and LS states, while under the influence of a polarized environment via a ferroelectric substrate, puts an energy change for this process at 110meV [63]. The change in conductance produces a noticeable sensing current contrast of two orders of magnitude between the HS and LS states on a transistor-like device structure, where state change, or spin state change is triggered by an external voltage. This gives a convincing demonstration for the use of molecular materials in a gated, voltage controlled spintronic device.

5. FUTURE WORK

The road to widespread use of organic spintronic devices could take many directions. Light emitting diodes and devices which use organic spin valves and magnetoresistance based on organic semi-conductors are the subject of much study [99]. Spin crossover materials offer many advantages over traditional silicon and metal oxide based devices [100], [101] such as low switching energy, small footprint, and GHz speed switching [102].

5.1 Device-based works

Due to technological demands and the nature of the spin crossover/ferroelectric structure's defining characteristics, it makes sense to further develop devices based of the platform presented in the preceding study. While many questions have been answered about the viability of molecular materials as device candidates, many yet remain.

5.1.1 Gated switchable molecular transistor: cycle repeatability, cycling time, and stability

One natural next step of this project is to develop a functioning molecular-based gated electronic device based on the already proven multiferroic properties of the $[Fe\{H_2B(pz)_2\}_2(bipy)]$ - PVDF-HFP system. This could be accomplished through the fabrication of a multilayered thin film construction like the device outlined in Figure 5.1. Cycling properties could be examined, including switching speed and stability. Ideally, this experiment would also incorporate some sort of spectroscopy, whether XAS or simple reflectance measurements, in order to capture the spin state transition along with conductance change. In fact, the glass MicruX sensor would be ideal for concurrent table top spectroscopy measurements and I-V curve characterization.

5.1.2 Addressing the local spin state of a molecular thin film: an integrated multiferroic array

One of the most appealing features of the SCO-ferroelectric multiferroic system is the possibility to address small, even molecule sized regions of the sample. This is an advantage

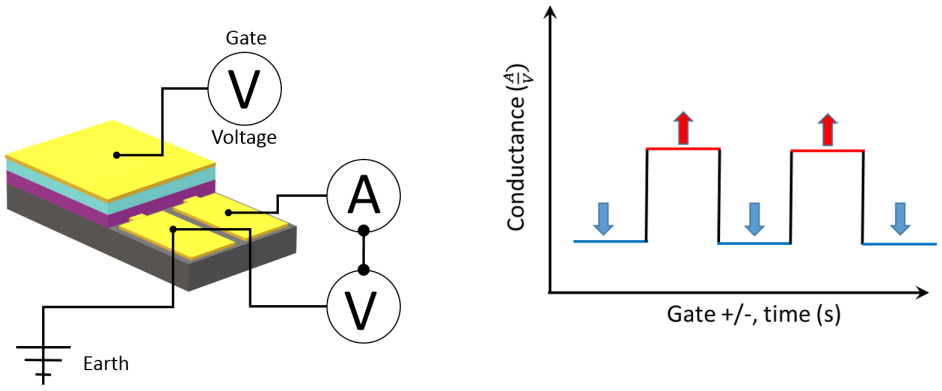

Figure 5.1. A proposed future device for demonstrating the viability of a SCO - ferroelectric molecular based gated electronic device. The device could be fabricated on a MicruX sensor in essentially the same manner as some of the devices already made for this study.

not only of molecular based magnetic materials, but also of the molecular ferroelectric. With the other mechanisms of spin state change, namely temperature, pressure, and light, it is very difficult to address specific areas of the sample. In fact these mechanisms exhibit a global influence on the system. Figure 5.2 shows a proposed experiment which could address nanoscaled regions across a SCO thin film, allowing for local control of the spin state of adjacent regions. This device would consist of a silicon substrate which would

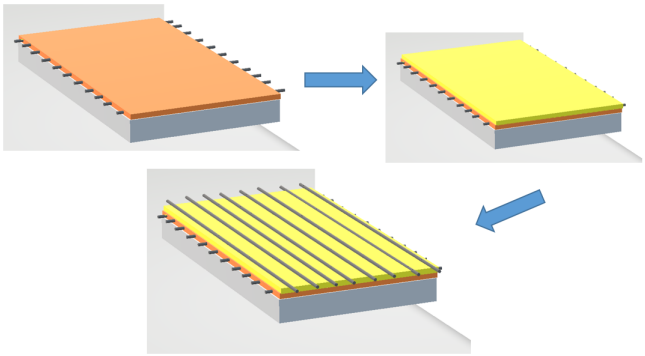

Figure 5.2. This figure shows a proposed structure for addressing the local spin state of a molecular thin film. The device is, in essence, an array of moleucular multiferroic gated devices. This would have direct application as a non-volatile memory device. Since $[Fe\{H_2B\,(pz)_2\}_2\,(bipy)]$ and PVDF-HFP are both soluble, they could be directly printed into such a configuration.

have a parallel array of conducting nanorods embedded in a ferroelectric PVDF based thin

film. A perpendicular array of conductive nanorods would then be formed across the top of the PVDF. Finally a SCO thin film of $[Fe\{H_2B(pz)_2\}_2(bipy)]$ would be deposited on top. Voltage could then be applied across an intersecting pair of nanorods, allowing for specific local control of the polarized environment of the SCO molecule.

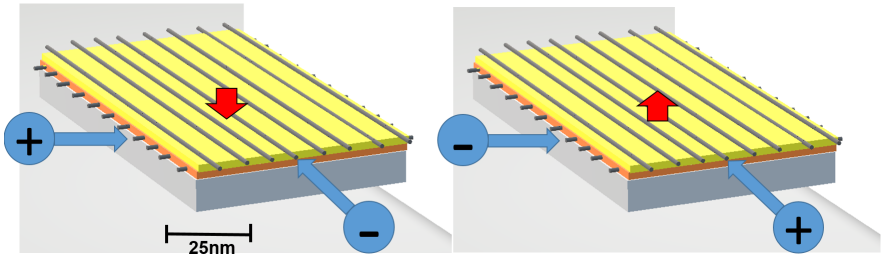

Figure 5.3. The completed device from Figure 5.2 would make it posible to address the local spin state of a surface by voltage control from the edge of the monolith.

The solubility and low toxicity of PVDF-HFP and $[Fe\{H_2B(pz)_2\}_2(bipy)]$ make them able to be directly printed onto an arrayed substrate. It is not beyond reason to expect that these devices could be made on demand, and pre-encoded with information, as an inexpensive way to carry data

5.2 Fundamental questions

In Figure 4.4, data shows that it is possible to lock a 65nm thin film of $[Fe\{H_2B(pz)_2\}_2(bipy)]$ into a mostly LS state past the it's transition temperature. In previous studies it was shown that the locking into the LS state was much more complete for thin films of just a few molecular layers, around 12nm thick [52]. This of course points to an interaction length, which was previously thought of to be much shorter than what has been observed here.

The environment that the molecule exists in while adsorbed to the surface of the ferroelectric, and the exact interactions at play during the spin state transition is not fully understood. Of course there is a change in the direction of the electric field that goes along with polarization reversal, but there is also a change in molecular conformation of the PVDF-HFP layer. The surface at the interface will terminate in hydrogen for an up polarization

and fluorine in a down polarization. It is possible that when adsorbed to the surface, the $[Fe\{H_2B\,(pz)_2\}_2\,(bipy)]$ molecule will have some preferential orientation, depending on the termination conformation at the interface. Steric hindrance of molecular rotation may contribute to the mechanics of the switching, and presently there is no direct evidence substrate polarization perturbation of the $[Fe\{H_2B\,(pz)_2\}_2\,(bipy)]$ spin states [63].

There have been claims of spin polarized current being produced due to the unpaired electrons in the HS state which are thought to be the main charge carriers [43]. An approach which uses spin polarized scanning tunneling microscopy may be able to directly probe the current for preferential spin, as well as the density of states using spin polarized scanning tunneling spectroscopy. A spin diode type device could possibly be fabricated.

REFERENCES

[1] H. Rohrer, "Limits and possibilities of miniaturization," *Japanese Journal of Applied Physics*, vol. 32, no. 3 S, 1993, ISSN: 13474065. DOI: 10.1143/JJAP.32.1335.

[2] R. W. Keyes, "Fundamental limits of silicon," *Proceedings of the IEEE*, vol. 89, no. 3, pp. 227–239, 2001, ISSN: 00189219. DOI: 10.1109/5.915372.

[3] S. Kumar, "Fundamental Limits to Moore ' s Law," pp. 1–3, 2015.

[4] W. Huang, K. Rajamani, M. R. Stan, and K. Skadron, "Scaling with design constraints: Predicting the future of big chips," *IEEE Micro*, vol. 31, no. 4, pp. 16–29, 2011, ISSN: 02721732. DOI: 10.1109/MM.2011.42.

[5] C. A. Mack, "Fifty Years of Moore's Law," *IEEE Transactions on Semiconductor Manufacturing*, vol. 24, no. 2, pp. 202–207, May 2011, ISSN: 0894-6507. DOI: 10.1109/TSM.2010.2096437. [Online]. Available: http://ieeexplore.ieee.org/document/5696765/.

[6] E. Pop, "Energy dissipation and transport in nanoscale devices," *Nano Research*, vol. 3, no. 3, pp. 147–169, Mar. 2010, ISSN: 1998-0124. DOI: 10.1007/s12274-010-1019-z. [Online]. Available: http://link.springer.com/10.1007/s12274-010-1019-z.

[7] S. Jan Van Der Molen and P. Liljeroth, "Charge transport through molecular switches," *Journal of Physics Condensed Matter*, vol. 22, no. 13, 2010, ISSN: 09538984. DOI: 10.1088/0953-8984/22/13/133001.

[8] A. Bousseksou, G. Molnár, L. Salmon, and W. Nicolazzi, "Molecular spin crossover phenomenon: Recent achievements and prospects," *Chemical Society Reviews*, vol. 40, no. 6, pp. 3313–3335, 2011, ISSN: 03060012. DOI: 10.1039/c1cs15042a. [Online]. Available: http://xlink.rsc.org/?DOI=c1cs15042a.

[9] P. Gütlich and H. A. Goodwin, "Spin Crossover—An Overall Perspective," in *Spin crossover in transition metal compunds I*, H. G. P. Gutlich, Ed., 1st ed., 2004, ch. 1, pp. 1–47, ISBN: 3-540-40394-9. DOI: 10.1007/b13527. [Online]. Available: http://www.springerlink.com/index/10.1007/b13527%20http://link.springer.com/10.1007/b13527.

[10] E. Konig and S. Kremer, "Exact spin-pairing energies at the crossovers in octahedral d 4, d 5, d 6, and d 7 transition metal complexes," *Theoretica Chimica Acta*, vol. 23, no. 1, pp. 12–20, 1971, ISSN: 0040-5744. DOI: 10.1007/BF00530196. [Online]. Available: http://link.springer.com/10.1007/BF00530196.

[11] K. Ridier, G. Molnár, L. Salmon, W. Nicolazzi, and A. Bousseksou, "Hysteresis, nucleation and growth phenomena in spin-crossover solids," *Solid State Sciences*, vol. 74, A1–A22, Dec. 2017, ISSN: 12932558. DOI: 10.1016/j.solidstatesciences.2017.10.014. [Online]. Available: https://www.sciencedirect.com/science/article/abs/pii/S1293255817309068?via%7B%5C%%7D3Dihub%20https://linkinghub.elsevier.com/retrieve/pii/S1293255817309068.

[12] J. A. Real, M. C. Muñoz, J. Faus, and X. Solans, "Spin Crossover in Novel Dihydrobis(1-pyrazolyl)borate [H ₂ B(pz) ₂]-Containing Iron(II) Complexes. Synthesis, X-ray Structure, and Magnetic Properties of [FeL{H ₂ B(pz) ₂ } ₂] (L = 1,10-Phenanthroli," *Inorganic Chemistry*, vol. 36, no. 14, pp. 3008–3013, 1997, ISSN: 0020-1669. DOI: 10.1021/ic960965c. [Online]. Available: http://pubs.acs.org/doi/abs/10.1021/ic960965c.

[13] N. Moliner, L. Salmon, L. Capes, M. C. Muñoz, J. F. Létard, A. Bousseksou, J. P. Tuchagues, J. J. McGarvey, A. C. Dennis, M. Castro, R. Burriel, and J. A. Real, "Thermal and optical switching of molecular spin states in the {[FeL[H2B(pz)2]2} spin-crossover system (L = bpy, phen)," *Journal of Physical Chemistry B*, vol. 106, no. 16, pp. 4276–4283, 2002, ISSN: 10895647. DOI: 10.1021/jp013872b.

[14] O. Kahn, *Molecular magnetism*. VCH, 1993, ISBN: 9781560815662. [Online]. Available: https://books.google.com/books?id=QwzwAAAAMAAJ.

[15] T. Palamarciuc, J. C. Oberg, F. El Hallak, C. F. Hirjibehedin, M. Serri, S. Heutz, J.-F. Létard, and P. Rosa, "Spin crossover materials evaporated under clean high vacuum and ultra-high vacuum conditions: from thin films to single molecules," *Journal of Materials Chemistry*, vol. 22, no. 19, p. 9690, 2012, ISSN: 0959-9428. DOI: 10.1039/c2jm15094h. [Online]. Available: http://xlink.rsc.org/?DOI=c2jm15094h.

[16] H. Naggert, A. Bannwarth, S. Chemnitz, T. von Hofe, E. Quandt, and F. Tuczek, "First observation of light-induced spin change in vacuum deposited thin films of iron spin crossover complexes," *Dalton Transactions*, vol. 40, no. 24, p. 6364, 2011, ISSN: 1477-9226. DOI: 10.1039/c1dt10651a. [Online]. Available: http://xlink.rsc.org/?DOI=c1dt10651a.

[17] S. Beniwal, X. Zhang, S. Mu, A. Naim, P. Rosa, G. Chastanet, J. F. Lï¿½tard, J. Liu, G. E. Sterbinsky, D. A. Arena, P. A. Dowben, and A. Enders, "Surface-induced spin state locking of the [Fe(H2B(pz)2)2(bipy)] spin crossover complex," *Journal of Physics Condensed Matter*, vol. 28, no. 20, 2016, ISSN: 1361648X. DOI: 10.1088/0953-8984/28/20/206002.

[18] X. Jiang, G. Hao, X. Wang, A. Mosey, X. Zhang, L. Yu, A. J. Yost, X. Zhang, A. D. DiChiara, A. T. N'Diaye, X. Cheng, J. Zhang, R. Cheng, X. Xu, and P. A. Dowben, "Tunable spin-state bistability in a spin crossover molecular complex," *Journal of*

Physics: Condensed Matter, vol. 31, no. 31, p. 315 401, Aug. 2019, ISSN: 0953-8984. DOI: 10.1088/1361-648X/ab1a7d. [Online]. Available: https://iopscience.iop.org/article/10.1088/1361-648X/ab1a7d.

[19] S. Palto, L. Blinov, A. Bune, E. Dubovik, V. Fridkin, N. Petukhova, K. Verkhovskaya, and S. Yudin, "Ferroelectric langmuir-blodgett films," *Ferroelectrics Letters Section*, vol. 19, no. 3-4, pp. 65–68, 1995, ISSN: 15635228. DOI: 10.1080/07315179508204276.

[20] S. Ducharme, T. Reece, C. Othon, and R. Rannow, "Ferroelectric polymer Langmuir-Blodgett films for nonvolatile memory applications," *IEEE Transactions on Device and Materials Reliability*, vol. 5, no. 4, pp. 720–735, Dec. 2005, ISSN: 1530-4388. DOI: 10.1109/TDMR.2005.860818. [Online]. Available: http://digitalcommons.unl.edu/cgi/viewcontent.cgi?article=1008%7B%5C&%7Dcontext=physicsfacpub%20http://ieeexplore.ieee.org/document/1573690/.

[21] S. Ducharme, V. M. Fridkin, A. V. Bune, S. P. Palto, L. M. Blinov, N. N. Petukhova, and S. G. Yudin, "Intrinsic Ferroelectric Coercive Field," *Physical Review Letters*, vol. 84, no. 1, pp. 175–178, Jan. 2000, ISSN: 0031-9007. DOI: 10.1103/PhysRevLett.84.175. [Online]. Available: https://link.aps.org/doi/10.1103/PhysRevLett.84.175.

[22] B. Stadlober, M. Zirkl, and M. Irimia-Vladu, "Route towards sustainable smart sensors: ferroelectric polyvinylidene fluoride-based materials and their integration in flexible electronics," *Chemical Society Reviews*, pp. 1787–1825, 2019, ISSN: 0306-0012. DOI: 10.1039/C8CS00928G. [Online]. Available: http://xlink.rsc.org/?DOI=C8CS00928G.

[23] R. Blinc and B. Žekš, "Dynamics of order-disorder-type ferroelectrics and antiferroelectrics," *Advances in Physics*, vol. 21, no. 93, pp. 693–757, 1972, ISSN: 14606976. DOI: 10.1080/00018737200101348.

[24] R. Hasegawa, Y. Takahashi, Y. Chatani, and H. Tadokoro, "Crystal Structures of Three Crystalline Forms of Poly(vinylidene fluoride)," *Polymer Journal*, vol. 3, no. 5, pp. 600–610, 1972, ISSN: 0032-3896. DOI: 10.1295/polymj.3.600.

[25] Y. L. Gal'perin, Y. V. Strogalin, and M. P. Mlenik, "Crystal structure of polyvinylidene fluoride," *Polymer Science U.S.S.R.*, vol. 7, no. 5, pp. 1031–1039, 1965, ISSN: 00323950. DOI: 10.1016/0032-3950(65)90032-8.

[26] K. Cai, M. Yang, H. Ju, S. Wang, Y. Ji, B. Li, K. W. Edmonds, Y. Sheng, B. Zhang, N. Zhang, S. Liu, H. Zheng, and K. Wang, "Electric field control of deterministic current-induced magnetization switching in a hybrid ferromagnetic/ferroelectric structure," *Nature Materials*, vol. 16, no. July, pp. 712–716, 2017, ISSN: 1476-1122. DOI: 10.1038/nmat4886. arXiv: 1604.05561. [Online]. Available: http://arxiv.org/abs/1604.05561%7B%5C%%7D5Cnhttp://www.nature.com/doifinder/10.1038/nmat4886.

[27] J. S. Humphrey and R. Amin-Sanayei, "Vinylidene Fluoride Polymers," *Encyclopedia of Polymer Science and Technology*, vol. 4, 2003. DOI: 10.1002/0471440264.pst392.

[28] Z. Yin, B. Tian, Q. Zhu, and C. Duan, "Characterization and application of PVDF and its copolymer films prepared by spin-coating and langmuir-blodgett method," *Polymers*, vol. 11, no. 12, 2019, ISSN: 20734360. DOI: 10.3390/polym11122033.

[29] J. Carvell and R. Cheng, "Study of electrical polarization hysteresis in ferroelectric polyvinylidene fluoride films," *Materials Letters*, vol. 64, no. 18, pp. 1992–1995, Sep. 2010, ISSN: 0167577X. DOI: 10.1016/j.matlet.2010.06.030. [Online]. Available: https://linkinghub.elsevier.com/retrieve/pii/S0167577X10004829.

[30] T. Furukawa, "Ferroelectric properties of vinylidene fluoride copolymers," *Phase Transitions*, vol. 18, no. January, 1989, pp. 143–211, 1989. [Online]. Available: https://doi.org/10.1080/01411598908206863.

[31] S. M. Nakhmanson, M. B. Nardelli, and J. Bernholc, "Collective polarization effects in β-polyvinylidene fluoride and its copolymers with tri- and tetrafluoroethylene," *Physical Review B - Condensed Matter and Materials Physics*, vol. 72, no. 11, pp. 1–8, 2005, ISSN: 10980121. DOI: 10.1103/PhysRevB.72.115210.

[32] Y. J. Yu and A. J. McGaughey, "Energy barriers for dipole moment flipping in PVDF-related ferroelectric polymers," *Journal of Chemical Physics*, vol. 144, no. 1, pp. 1–7, 2016, ISSN: 00219606. DOI: 10.1063/1.4939152. [Online]. Available: http://dx.doi.org/10.1063/1.4939152.

[33] R. C. Ferguson, "Structural and Compositional Analysis of Vinylidene Fluoride-Hexafluoropropylene Copolymers by Nuclear Magnetic Resonance Spectroscopy," *Journal of the American Chemical Society*, vol. 82, no. 10, pp. 2416–2418, 1960, ISSN: 15205126. DOI: 10.1021/ja01495a003.

[34] A. C. Jayasuriya, A. Schirokauer, and J. I. Scheinbeim, "Crystal-structure dependence of electroactive properties in differently prepared poly(vinylidene fluoride/hexafluoropropylene) copolymer films," *Journal of Polymer Science, Part B: Polymer Physics*, vol. 39, no. 22, pp. 2793–2799, 2001, ISSN: 08876266. DOI: 10.1002/polb.10035.

[35] S. Dixon, D. R. Rexford, and J. S. Rugg, "Vinylidene Fluoride – Hexafluoropropylene Copolymer," *Industrial & Engineering Chemistry*, vol. 49, no. 10, pp. 1687–1690, 2005, ISSN: 0019-7866. DOI: 10.1021/ie50574a025.

[36] J. Wang, F. Guan, Q. Wang, L. Zhu, and J. Pan, " Crystal Orientation Effect on Electric Energy Storage in Poly(vinylidene fluoride- co -hexafluoropropylene) Copolymers," *Macromolecules*, vol. 43, no. 1, pp. 384–392, 2009, ISSN: 0024-9297. DOI: 10.1021/ma901921h.

[37] X. He, K. Yao, and B. K. Gan, "Phase transition and properties of a ferroelectric poly(vinylidene fluoride-hexafluoropropylene) copolymer," *Journal of Applied Physics*, vol. 97, no. 8, 2005, ISSN: 00218979. DOI: 10.1063/1.1862323.

[38] T. Bučko, J. Hafner, S. Lebègue, and J. G. Ángyán, "Spin crossover transition of Fe(phen)2(NCS)2: Periodic dispersion-corrected density-functional study," *Physical Chemistry Chemical Physics*, vol. 14, no. 16, pp. 5389–5396, 2012, ISSN: 14639076. DOI: 10.1039/c2cp40111h.

[39] K. Tarafder, S. Kanungo, P. M. Oppeneer, and T. Saha-Dasgupta, "Pressure and temperature control of spin-switchable metal-organic coordination polymers from ab initio calculations," *Physical Review Letters*, vol. 109, no. 7, pp. 1–5, 2012, ISSN: 00319007. DOI: 10.1103/PhysRevLett.109.077203.

[40] C. De Graaf and C. Sousa, "Study of the light-Induced spin crossover process of the [FeII(bpy)3]2+complex," *Chemistry - A European Journal*, vol. 16, no. 15, pp. 4550–4556, 2010, ISSN: 09476539. DOI: 10.1002/chem.200903423. arXiv: 0610288 [physics].

[41] S. Song, M. C. Kim, E. Sim, A. Benali, O. Heinonen, and K. Burke, "Benchmarks and Reliable DFT Results for Spin Gaps of Small Ligand Fe(II) Complexes," *Journal of Chemical Theory and Computation*, vol. 14, no. 5, pp. 2304–2311, 2018, ISSN: 15499626. DOI: 10.1021/acs.jctc.7b01196.

[42] M. Fumanal, L. K. Wagner, S. Sanvito, and A. Droghetti, "Diffusion Monte Carlo Perspective on the Spin-State Energetics of [Fe(NCH)6]2+," *Journal of Chemical Theory and Computation*, vol. 12, no. 9, pp. 4233–4241, 2016, ISSN: 15499626. DOI: 10.1021/acs.jctc.6b00332.

[43] D. Aravena and E. Ruiz, "Coherent Transport through Spin-Crossover Single Molecules," *Journal of the American Chemical Society*, vol. 134, no. 2, pp. 777–779, Jan. 2012, ISSN: 0002-7863. DOI: 10.1021/ja2090096. [Online]. Available: https://pubs.acs.org/doi/10.1021/ja2090096.

[44] T. Miyamachi, M. Gruber, V. Davesne, M. Bowen, S. Boukari, L. Joly, F. Scheurer, G. Rogez, T. K. Yamada, P. Ohresser, E. Beaurepaire, and W. Wulfhekel, "Robust spin crossover and memristance across a single molecule," *Nature Communications*, vol. 3, no. 1, p. 938, Jan. 2012, ISSN: 2041-1723. DOI: 10.1038/ncomms1940. [Online]. Available: http://www.nature.com/articles/ncomms1940.

[45] V. Meded, A. Bagrets, K. Fink, R. Chandrasekar, M. Ruben, F. Evers, A. Bernand-Mantel, J. S. Seldenthuis, A. Beukman, and H. S. Van Der Zant, "Electrical control over the Fe(II) spin crossover in a single molecule: Theory and experiment," *Physical Review B - Condensed Matter and Materials Physics*, vol. 83, no. 24, pp. 1–13, 2011, ISSN: 10980121. DOI: 10.1103/PhysRevB.83.245415.

[46] D. Gatteschi, L. Bogani, A. Cornia, M. Mannini, L. Sorace, and R. Sessoli, "Molecular magnetism, status and perspectives," *Solid State Sciences*, vol. 10, no. 12, pp. 1701–1709, 2008, ISSN: 12932558. DOI: 10.1016/j.solidstatesciences.2008.03.013. [Online]. Available: http://dx.doi.org/10.1016/j.solidstatesciences.2008.03.013.

[47] N. Baadji and S. Sanvito, "Giant resistance change across the phase transition in spin-crossover molecules," *Physical Review Letters*, vol. 108, no. 21, pp. 1–5, 2012, ISSN: 00319007. DOI: 10.1103/PhysRevLett.108.217201. arXiv: 1201.2028.

[48] L. Cambi and L. Szegö, "Über die magnetische Susceptibilität der komplexen Verbindungen (II. Mitteil.).," *Berichte der deutschen chemischen Gesellschaft (A and B Series)*, vol. 66, no. 5, pp. 656–661, May 1933, ISSN: 03659488. DOI: 10.1002/cber.19330660508. [Online]. Available: https://onlinelibrary.wiley.com/doi/abs/10.1002/cber.19330660508%20http://doi.wiley.com/10.1002/cber.19330660508.

[49] H. A. Bethe, "Splitting of Terms in Crystals," *Ann. Physik*, vol. 3, pp. 133–206, 1929, ISSN: 9789264223998 (PDF). DOI: 10.1787/key_energ_stat-2014-en. [Online]. Available: http://www.iea.org/publications/freepublications/publication/KeyWorld2014.pdf.

[50] E. Konig and K. Madeja, "5T2-1A1 Equilibriums in some iron(II)-bis(1,10-phenanthroline) complexes," *Inorganic Chemistry*, vol. 6, no. 1, pp. 48–55, 1967, ISSN: 1520510X. DOI: 10.1021/ic50047a011.

[51] B. Warner, J. C. Oberg, T. G. Gill, F. El Hallak, C. F. Hirjibehedin, M. Serri, S. Heutz, M.-A. Arrio, P. Sainctavit, M. Mannini, G. Poneti, R. Sessoli, and P. Rosa, "Temperature- and Light-Induced Spin Crossover Observed by X-ray Spectroscopy on Isolated Fe(II) Complexes on Gold," *The Journal of Physical Chemistry Letters*, vol. 4, no. 9, pp. 1546–1552, May 2013, ISSN: 1948-7185. DOI: 10.1021/jz4005619. [Online]. Available: https://pubs.acs.org/doi/10.1021/jz4005619.

[52] X. Zhang, T. Palamarciuc, J.-F. F. Létard, P. Rosa, E. V. Lozada, F. Torres, L. G. Rosa, B. Doudin, and P. A. Dowben, "The spin state of a molecular adsorbate driven by the ferroelectric substrate polarization," *Chemical Communications*, vol. 50, no. 18, p. 2255, 2014, ISSN: 13597345. DOI: 10.1039/c3cc46892e. [Online]. Available: http://xlink.rsc.org/?DOI=c3cc46892e.

[53] G. Rojas, X. Chen, C. Bravo, J. H. Kim, J. S. Kim, J. Xiao, P. A. Dowben, Y. Gao, X. C. Zeng, W. Choe, and A. Enders, "Self-assembly and properties of nonmetalated tetraphenyl-porphyrin on metal substrates," *Journal of Physical Chemistry C*, vol. 114, no. 20, pp. 9408–9415, 2010, ISSN: 19327447. DOI: 10.1021/jp1012957.

[54] G. Rojas, S. Simpson, X. Chen, D. A. Kunkel, J. Nitz, J. Xiao, P. A. Dowben, E. Zurek, and A. Enders, "Surface state engineering of molecule-molecule interactions," *Physical Chemistry Chemical Physics*, vol. 14, no. 14, pp. 4971–4976, 2012, ISSN: 14639076. DOI: 10.1039/c2cp40254h.

[55] P. A. Dowben, L. G. Rosa, C. C. Ilie, and J. Xiao, "Adsorbate/absorbate interactions with organic ferroelectric polymers," *Journal of Electron Spectroscopy and Related Phenomena*, vol. 174, no. 1-3, pp. 10–21, 2009, ISSN: 03682048. DOI: 10.1016/j.elspec.2009.03.005.

[56] T. G. Gopakumar, M. Bernien, H. Naggert, F. Matino, C. F. Hermanns, A. Bannwarth, S. Mühlenberend, A. Krüger, D. Krüger, F. Nickel, W. Walter, R. Berndt, W. Kuch, and F. Tuczek, "Spin-crossover complex on Au(111): Structural and electronic differences between mono- and multilayers," *Chemistry - A European Journal*, vol. 19, no. 46, pp. 15 702–15 709, 2013, ISSN: 09476539. DOI: 10.1002/chem.201302241.

[57] X. Zhang, P. S. Costa, J. Hooper, D. P. Miller, A. T. N'Diaye, S. Beniwal, X. Jiang, Y. Yin, P. Rosa, L. Routaboul, M. Gonidec, L. Poggini, P. Braunstein, B. Doudin, X. Xu, A. Enders, E. Zurek, and P. A. Dowben, "Locking and Unlocking the Molecular Spin Crossover Transition," *Advanced Materials*, vol. 29, no. 39, pp. 1–10, 2017, ISSN: 15214095. DOI: 10.1002/adma.201702257.

[58] Y. Zhang, "Driving spin transition at interface: Role of adsorption configurations," *Journal of Chemical Physics*, vol. 148, no. 4, 2018, ISSN: 00219606. DOI: 10.1063/1.5007739.

[59] C. Lefter, R. Tan, S. Tricard, J. Dugay, G. Molnár, L. Salmon, J. Carrey, A. Rotaru, and A. Bousseksou, "On the stability of spin crossover materials: From bulk samples to electronic devices," *Polyhedron*, vol. 102, pp. 434–440, 2015, ISSN: 02775387. DOI: 10.1016/j.poly.2015.10.021. [Online]. Available: http://dx.doi.org/10.1016/j.poly.2015.10.021.

[60] H. Jeong, D. Kim, D. Xiang, and T. Lee, "High-Yield Functional Molecular Electronic Devices," *ACS Nano*, vol. 11, no. 7, pp. 6511–6548, 2017, ISSN: 1936086X. DOI: 10.1021/acsnano.7b02967.

[61] T. M. Dunn, D. S. McClure, and R. G. Pearson., *Some Aspects of Crystal Field Theory*. Harper, 1965.

[62] C. J. Ballhausen, *Introduction to ligand field theory*. McGraw-Hill, 1962.

[63] A. Mosey, A. S. Dale, G. Hao, A. N'Diaye, P. A. Dowben, and R. Cheng, "Quantitative Study of the Energy Changes in Voltage-Controlled Spin Crossover Molecular Thin Films," *The Journal of Physical Chemistry Letters*, vol. 11, no. 19, pp. 8231–8237,

Oct. 2020, ISSN: 1948-7185. DOI: 10.1021/acs.jpclett.0c02209. [Online]. Available: https://pubs.acs.org/doi/10.1021/acs.jpclett.0c02209.

[64] A. Bousseksou, J. Nasser, J. Linares, K. Boukheddaden, F. Varret, A. Bousseksou, J. Nasser, J. Linares, K. Boukheddaden, and F. V. Ising-like, "Ising-like model for the two-step spin-crossover," *Journal de Physique I*, vol. 2, no. 7, pp. 1381–1403, 1992.

[65] A. Bousseksou and G. Molnár, "The spin-crossover phenomenon: towards molecular memories," *Comptes Rendus Chimie*, vol. 6, no. 8-10, pp. 1175–1183, Aug. 2003, ISSN: 16310748. DOI: 10.1016/j.crci.2003.08.011. [Online]. Available: https://linkinghub.elsevier.com/retrieve/pii/S1631074803001863.

[66] G. D'Avino, A. Painelli, and K. Boukheddaden, "Vibronic model for spin crossover complexes," *Physical Review B*, vol. 84, no. 10, p. 104 119, Sep. 2011, ISSN: 1098-0121. DOI: 10.1103/PhysRevB.84.104119. [Online]. Available: https://link.aps.org/doi/10.1103/PhysRevB.84.104119.

[67] C. Jureschi, J. Linares, A. Rotaru, and Y. Garcia, "Multi-Step in 3D Spin Crossover Nanoparticles Simulated by an Ising Model Using Entropic Sampling Monte Carlo Technique," *Magnetochemistry*, vol. 2, no. 1, p. 13, 2016, ISSN: 2312-7481. DOI: 10.3390/magnetochemistry2010013.

[68] D. Chiruta, J. Linares, M. Dimian, Y. Alayli, and Y. Garcia, "Role of edge atoms in the hysteretic behaviour of 3D spin crossover nanoparticles revealed by an Ising-like model," *European Journal of Inorganic Chemistry*, no. 29, pp. 5086–5093, 2013, ISSN: 14341948. DOI: 10.1002/ejic.201300757.

[69] N. W. Ashcroft and N. D. Mermin, *Solid State Physics*, ser. HRW international editions. Holt, Rinehart and Winston, 1976, ISBN: 9780030839931. [Online]. Available: https://books.google.com/books?id=1C9HAQAAIAAJ.

[70] X. Zhang, T. Palamarciuc, P. Rosa, B. Doudin, Z. Zhang, J. Wang, P. A. Dowben, J.-F. Létard, B. Doudin, Z. Zhang, J. Wang, and P. A. Dowben, "Electronic Structure of a Spin Crossover Molecular Adsorbate," *The Journal of Physical Chemistry C*, vol. 116, no. 44, pp. 23 291–23 296, Nov. 2012, ISSN: 1932-7447. DOI: 10.1021/jp3034962. [Online]. Available: https://pubs.acs.org/doi/10.1021/jp3034962.

[71] S. Ducharme, "Ferroelectric polymer Langmuir-Blodgett films," in *Handbook of Thin FIlms*, H. S. Nalwa, Ed., Academic Press, 2002, ch. 11, p. 3444, ISBN: 978-0-12-512908-4.

[72] Z. Zhang, R. González, G. Díaz, L. G. Rosa, I. Ketsman, X. Zhang, P. Sharma, A. Gruverman, and P. A. Dowben, "Polarization mediated chemistry on ferroelectric polymer surfaces," *Journal of Physical Chemistry C*, vol. 115, no. 26, pp. 13 041–13 046, 2011, ISSN: 19327447. DOI: 10.1021/jp203544k.

[73] M. Celestin, S. Krishnan, S. Bhansali, E. Stefanakos, and D. Y. Goswami, "A review of self-assembled monolayers as potential terahertz frequency tunnel diodes," *Nano Research*, vol. 7, no. 5, pp. 589–625, 2014, ISSN: 19980000. DOI: 10.1007/s12274-014-0429-8.

[74] F. Hippert, E. Geissler, J. L. Hodeau, E. Lelièvre-Berna, and J. R. Regnard, *Neutron and X-ray Spectroscopy*, ser. Grenoble sciences. Springer Netherlands, 2005, ISBN: 9781402033360. [Online]. Available: https://books.google.com/books?id=C03N3xu8UWUC.

[75] P. Willmott, *An introduction to synchrotron radiation*, 1st ed. John Wiley and Sons, 2011, p. 352, ISBN: 978-0-470-74578-6.

[76] B. H. Bransden, C. J. Joachain, and T. J. Plivier, *Physics of Atoms and Molecules*, ser. Pearson Education. Prentice Hall, 2003, ISBN: 9780582356924. [Online]. Available: https://books.google.com/books?id=ST%7B%5C_%7DDwIGZeTQC.

[77] X. Zhang, S. Mu, G. Chastanet, N. Daro, T. Palamarciuc, P. Rosa, J. F. Létard, J. Liu, G. E. Sterbinsky, D. A. Arena, C. Etrillard, B. Kundys, B. Doudin, and P. A. Dowben, "Complexities in the molecular spin crossover transition," *Journal of Physical Chemistry C*, vol. 119, no. 28, pp. 16 293–16 302, 2015, ISSN: 19327455. DOI: 10.1021/acs.jpcc.5b02220.

[78] P. Nachimuthu, J. H. Underwood, C. D. Kemp, E. M. Gullikson, D. W. Lindle, D. K. Shuh, and R. C. Perera, "Performance characteristics of beamline 6.3.1 from 200 ev to 2000 ev at the advanced light source," *AIP Conference Proceedings*, vol. 705, pp. 454–457, 2004, ISSN: 15517616. DOI: 10.1063/1.1757832.

[79] G. Hao, A. Mosey, X. Jiang, A. J. Yost, K. R. Sapkota, G. T. Wang, X. Zhang, J. Zhang, A. T. N'Diaye, R. Cheng, X. Xu, and P. A. Dowben, "Nonvolatile voltage controlled molecular spin state switching," *Applied Physics Letters*, vol. 114, no. 3, p. 032 901, Jan. 2019, ISSN: 00036951. DOI: 10.1063/1.5054909. [Online]. Available: http://aip.scitation.org/doi/10.1063/1.5054909.

[80] W. Zhang, R. Alonso-Mori, U. Bergmann, C. Bressler, M. Chollet, A. Galler, W. Gawelda, R. G. Hadt, R. W. Hartsock, T. Kroll, K. S. Kjær, K. Kubiek, H. T. Lemke, H. W. Liang, D. A. Meyer, M. M. Nielsen, C. Purser, J. S. Robinson, E. I. Solomon, Z. Sun, D. Sokaras, T. B. Van Driel, G. Vankó, T. C. Weng, D. Zhu, and K. J. Gaffney, "Tracking excited-state charge and spin dynamics in iron coordination complexes," *Nature*, vol. 509, no. 7500, pp. 345–348, 2014, ISSN: 14764687. DOI: 10.1038/nature13252. [Online]. Available: http://www.nature.com/doifinder/10.1038/nature13252.

[81] S. L. Schroeder, G. D. Moggridge, R. M. Ormerod, T. Rayment, and R. M. Lambert, "What determines the probing depth of electron yield XAS?" *Surface Science*, vol. 324, no. 2-3, 1995, ISSN: 00396028. DOI: 10.1016/0039-6028(94)00779-9.

[82] S. L. Schroeder, "Towards a 'universal curve' for total electron-yield XAS," *Solid State Communications*, vol. 98, no. 5, pp. 405–409, 1996, ISSN: 00381098. DOI: 10.1016/0038-1098(96)00035-X.

[83] A. Erbil, G. S. Cargill, R. Frahm, and R. F. Boehme, "Total-electron-yield current measurements for near-surface extended x-ray-absorption fine structure," *Physical Review B*, vol. 37, no. 5, pp. 2450–2464, 1988, ISSN: 01631829. DOI: 10.1103/PhysRevB.37.2450.

[84] L. Salmon, G. Molnár, S. Cobo, P. Oulié, M. Etienne, T. Mahfoud, P. Demont, A. Eguchi, H. Watanabe, K. Tanaka, and A. Bousseksou, "Re-investigation of the spin crossover phenomenon in the ferrous complex [Fe(HB(pz)3)2]," *New Journal of Chemistry*, vol. 33, no. 6, p. 1283, 2009, ISSN: 1144-0546. DOI: 10.1039/b902811k. [Online]. Available: http://xlink.rsc.org/?DOI=b902811k.

[85] C. Faulmann, K. Jacob, S. Dorbes, S. Lampert, I. Malfant, M.-L. L. Doublet, L. Valade, and J. A. Real, "Electrical conductivity and spin crossover: A new achievement with a metal bis dithiolene complex," *Inorganic Chemistry*, vol. 46, no. 21, pp. 8548–8559, Oct. 2007, ISSN: 00201669. DOI: 10.1021/ic062461c. [Online]. Available: https://pubs.acs.org/doi/10.1021/ic062461c.

[86] A. Rotaru, I. A. Gural'Skiy, G. Molnár, L. Salmon, P. Demont, and A. Bousseksou, "Spin state dependence of electrical conductivity of spin crossover materials," *Chemical Communications*, vol. 48, no. 35, pp. 4163–4165, 2012, ISSN: 13597345. DOI: 10.1039/c2cc30528c.

[87] Y.-S. Koo and J. R. Galán-Mascarós, "Spin Crossover Probes Confer Multistability to Organic Conducting Polymers," *Advanced Materials*, vol. 26, no. 39, pp. 6785–6789, 2014. DOI: 10.1002/adma.201402579.

[88] J. Dugay, M. Aarts, M. Giménez-Marqués, T. Kozlova, H. W. Zandbergen, E. Coronado, and H. S. J. van der Zant, "Phase Transitions in Spin-Crossover Thin Films Probed by Graphene Transport Measurements," *Nano Letters*, vol. 17, no. 1, pp. 186–193, Jan. 2017, ISSN: 1530-6984. DOI: 10.1021/acs.nanolett.6b03780. arXiv: 1609.04738. [Online]. Available: https://pubs.acs.org/doi/10.1021/acs.nanolett.6b03780.

[89] C. Lefter, S. Rat, J. S. Costa, M. D. Manrique-Juárez, C. M. Quintero, L. Salmon, I. Séguy, T. Leichle, L. Nicu, P. Demont, A. Rotaru, G. Molnár, and A. Bousseksou, "Current Switching Coupled to Molecular Spin-States in Large-Area Junctions,"

Advanced Materials, vol. 28, no. 34, pp. 7508–7514, 2016. DOI: 10.1002/adma.201601420.

[90] J. Dugay, M. Giménez-Marqués, T. Kozlova, H. W. Zandbergen, E. Coronado, and H. S. J. Van Der Zant, "Spin switching in electronic devices based on 2D assemblies of spin-crossover nanoparticles," *Advanced Materials*, vol. 27, no. 7, pp. 1288–1293, 2015, ISSN: 15214095. DOI: 10.1002/adma.201404441. arXiv: 1412.1345.

[91] Y. Zhang, I. Séguy, K. Ridier, V. Shalabaeva, M. Piedrahita-Bello, A. Rotaru, L. Salmon, G. Molnár, and A. Bousseksou, "Resistance switching in large-area vertical junctions of the molecular spin crossover complex [Fe(HB(tz)3)2]: ON/OFF ratios and device stability," *Journal of Physics Condensed Matter*, vol. 32, no. 21, 2020, ISSN: 1361648X. DOI: 10.1088/1361-648X/ab741e.

[92] Keithley, *Low Level Measurements Handbook- Precision DC current, voltage and resistance measurements.* 2004, p. 239.

[93] R. Manual, *Model 6487 Picoammeter / Voltage Source Reference Manual Model 6487 Picoammeter / Voltage Source Reference Manual*, March. 2011.

[94] G. Hao, R. Cheng, and P. A. Dowben, "The emergence of the local moment molecular spin transistor," *Journal of Physics Condensed Matter*, vol. 32, no. 23, 2020, ISSN: 1361648X. DOI: 10.1088/1361-648X/ab74e4.

[95] S. Maji, P. K. Sarkar, L. Aggarwal, S. K. Ghosh, D. Mandal, G. Sheet, and S. Acharya, "Self-oriented β-crystalline phase in the polyvinylidene fluoride ferroelectric and piezo-sensitive ultrathin Langmuir–Schaefer film," *Physical Chemistry Chemical Physics*, vol. 17, no. 12, pp. 8159–8165, 2015, ISSN: 1463-9076. DOI: 10.1039/C5CP00218D. [Online]. Available: http://dx.doi.org/10.1039/C5CP00218D%20http://xlink.rsc.org/?DOI=C5CP00218D.

[96] A. K. Tagantsev, I. Stolichnov, E. L. Colla, and N. Setter, "Polarization fatigue in ferroelectric films: Basic experimental findings, phenomenological scenarios, and microscopic features," *Journal of Applied Physics*, vol. 90, no. 3, pp. 1387–1402, Aug. 2001, ISSN: 0021-8979. DOI: 10.1063/1.1381542. [Online]. Available: http://aip.scitation.org/doi/10.1063/1.1381542.

[97] M. Cinchetti, V. A. Dediu, and L. E. Hueso, "Activating the molecular spinterface," *Nature Materials*, vol. 16, no. 5, pp. 507–515, May 2017, ISSN: 1476-1122. DOI: 10.1038/nmat4902. [Online]. Available: http://www.nature.com/doifinder/10.1038/nmat4902%20http://www.nature.com/articles/nmat4902.

[98] E. Ruiz, "Charge transport properties of spin crossover systems," *Physical Chemistry Chemical Physics*, vol. 16, no. 1, pp. 14–22, 2014, ISSN: 14639076. DOI: 10.1039/c3cp54028f.

[99] R. Geng, H. M. Luong, T. T. Daugherty, L. Hornak, and T. D. Nguyen, "A review on organic spintronic materials and devices: II. Magnetoresistance in organic spin valves and spin organic light emitting diodes," *Journal of Science: Advanced Materials and Devices*, vol. 1, no. 3, pp. 256–272, 2016, ISSN: 24682179. DOI: 10.1016/j.jsamd.2016.08.006. [Online]. Available: http://dx.doi.org/10.1016/j.jsamd.2016.08.006.

[100] C. Lefter, R. Tan, J. Dugay, S. Tricard, G. Molnár, L. Salmon, J. Carrey, W. Nicolazzi, A. Rotaru, and A. Bousseksou, "Unidirectional electric field-induced spin-state switching in spin crossover based microelectronic devices," *Chemical Physics Letters*, vol. 644, pp. 138–141, Jan. 2016, ISSN: 00092614. DOI: 10.1016/j.cplett.2015.11.036. [Online]. Available: http://dx.doi.org/10.1016/j.cplett.2015.11.036%20https://linkinghub.elsevier.com/retrieve/pii/S0009261415008878.

[101] K. Senthil Kumar and M. Ruben, "Emerging trends in spin crossover (SCO) based functional materials and devices," *Coordination Chemistry Reviews*, vol. 346, pp. 176–205, Sep. 2017, ISSN: 00108545. DOI: 10.1016/j.ccr.2017.03.024.

[102] J. Trasobares, D. Vuillaume, D. Théron, and N. Clément, "A 17 GHz molecular rectifier," *Nature Communications*, vol. 7, no. 1, p. 12 850, Nov. 2016, ISSN: 2041-1723. DOI: 10.1038/ncomms12850. [Online]. Available: http://www.nature.com/articles/ncomms12850.